1661-8726/07/010085-23
DOI 10.1007/s00015-007-1203-7
Birkhäuser Verlag, Basel, 2007

Swiss j. geosci. 100 (2007) 85–107

Age and isotopic constraints on magmatism along the Karakoram-Kohistan Suture Zone, NW Pakistan: evidence for subduction and continued convergence after India-Asia collision

Stefan Heuberger[1], Urs Schaltegger [2,3], Jean-Pierre Burg[1], Igor Maria Villa[4,5], Martin Frank[3,6], Hamid Dawood[7], Shahid Hussain[7] & Andrea Zanchi[5]

Key words: Suture zone, collision, arc magmatism, geochronology, Karakoram, Kohistan

ABSTRACT

Detailed geological mapping in the Drosh-Shishi area in southern Chitral (NW Pakistan) was combined with high-precision U-Pb dating on zircons to constrain the timing of magmatism and associated deformation/metamorphic events related to the Kohistan-Karakoram convergence and collision. Our new ages indicate that the Mesozoic to Tertiary magmatic history of this region is influenced by long-lived melt generation above an active subduction zone. Dated intrusive rocks range in age from 130 to 39 million years, indicating that subduction-related magmatism continued after the Kohistan-Karakoram and the India-Asia collisions. Initial hafnium isotope ratios were measured on the dated zircons to constrain the type of melt source of the dated plutons. The data reveal the different nature of partly coeval magmatism in these units, i.e. continental arc magmatism in the Karakoram (ca. 130-104 Ma) and arc magmatism on the Kohistan side (112-39 Ma). Intrusions within the suture zone can be clearly traced to be Karakoram-derived on the basis of initial Hf isotopic compositions. Granite dykes crosscutting the Kohistan units have sampled an underlying, old continental basement of Gondwana affinity. The geochronological evidence presented in this paper is consistent with Cretaceous subduction beneath the Karakoram Terrane. The related calc-alkaline magmatism seems to have stopped at about 100 Ma. Granite dykes on the Kohistan side show that the magmatic and tectonic history of the Karakoram-Kohistan Suture Zone continued to the Eocene. This long tectono-metamorphic and magmatic activity in the arc plates was likely due to complex and few million year long interplays between subduction and thrusting events in the forearc, within-arc and back-arc regions between two active subduction zones.

Introduction – Geological setting

The Karakoram-Kohistan Suture Zone (KKSZ) is the northern branch of the western continuations of the Yalu-Tsangpo Suture recognised in southern Tibet (e.g. Gansser, 1980). The KKSZ separates in NW Pakistan the Karakoram Terrane, to the north, from the Kohistan Paleo-Island Arc Complex, to the south. It becomes eastward the Shyok Suture, which separates the Ladakh Arc from the Karakoram Terrane (Honegger et al., 1982), a former fragment of Gondwana that started drifting northward during the Permian and accreted to Asia before the Mid-Cretaceous (Boulin, 1981; Tapponnier et al., 1981). We reserve the name Main Karakoram Thrust, sometimes employed in the literature to describe the Karakoram-Kohistan Suture, for the thrust that places high-grade metamorphic rocks onto low-grade, likely Paleozoic rocks within the Karakoram Terrane (e.g., Searle et al. 1999). This denomina-

[1] Institute of Geology, ETH- and University of Zürich, Sonneggstrasse 5, 8092 Zürich, Switzerland. E-mail: stefan.heuberger@alumni.ethz.ch
[2] Département de Minéralogie, Université de Genève, rue des Maraîchers 13, 1205 Genève, Switzerland. E-mail: Urs.Schaltegger@terre.unige.ch
[3] Institute of Isotope Geology and Mineral Resources, ETH Zürich, Sonneggstr. 5, 8092 Zürich, Switzerland. E-mail: jean-pierre.burg@erdw.ethz.ch
[4] Institut für Geologie, University of Bern, Baltzerstrasse 1, 3012 Bern, Switzerland. E-mail: villa@geo.unibe.ch
[5] Dipartimento di Scienze Geologiche e Geotecnologie, Università di Milano Bicocca, 20126 Milano, Italy. E-mail: andrea.zanchi@unimib.it
[6] present address: IfM-GEOMAR, Leibniz Institute for Marine Sciences at the University of Kiel, Wischhofstrasse 1–3, 24148 Kiel, Germany. E-mail: mfrank@ifm-geomar.de.
[7] Pakistan Museum of Natural History, Garden Avenue, Shakarparian, Islamabad 44000, Pakistan. E-mail: pmnh@esdpmnh.isb.sdnpk.org

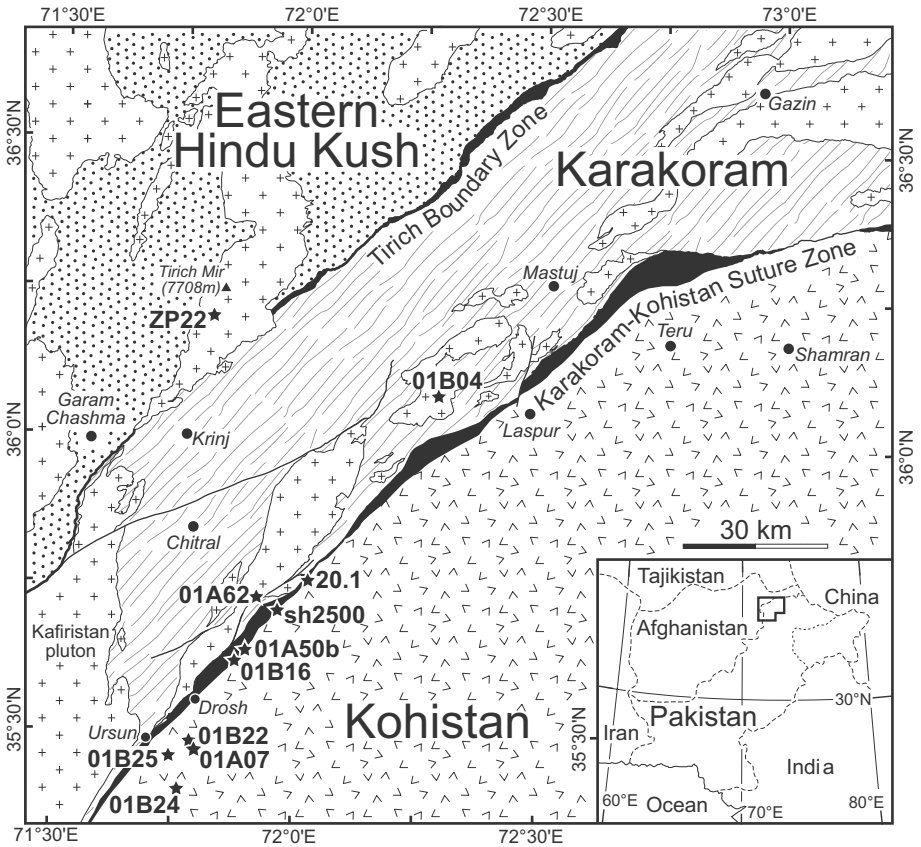

Fig. 1. Structural sketch map of the Chitral district, NW Pakistan, with location of the dated samples. Based on Landsat ETM+ image no. 150-035, modified maps by Pudsey, 1986; Pudsey et al., 1985a; Gaetani et al., 1996; Hildebrand et al., 2001; Zanchi et al., 2000 and own field work.

tion hence becomes consistent with the appellation of Main Central Thrust applied to the within-India thrust zone that places high-grade metamorphic rocks onto lower-grade sequences (e.g., Gansser, 1964). The Kohistan and Ladakh arcs developed in the Mesozoic above a north-dipping subduction zone within the Tethys Ocean (e.g. Tahirkheli et al., 1979; Bard et al., 1980; Dietrich et al., 1983 and many authors after them). Both arcs are now squeezed between the Indian and Asian continental plates.

Our work focuses on the 125 km long, SW-NE trending segment of the KKSZ in the Chitral area, from Ursun to Laspur (Fig. 1). The KKSZ along this stretch is a 1–7 km wide fault zone in which imbricate lithologies belong to the three tectonic units, from NW to SE: (1) the former Karakoram active margin, (2) the North-Tethys Ocean (oceanic back-arc basin?) and (3) the Kohistan Paleo-Island Arc (Heuberger, 2004). Complex imbrication led earlier authors to describe the KKSZ as a "mélange" zone formed in a small back-arc basin (Khan et al., 1996; Pudsey, 1986; Pudsey et al., 1985a) which closed between 100 and 75 Ma (Petterson and Windley, 1985; Treloar et al., 1989 and later authors). In our field area, similar apatite ages on both sides of the suture show that the rocks on either side passed the apatite partial annealing zone together, around 11-13 Ma (work in progress); accordingly, no or little vertical differential movement has taken place along this fault zone since the late Miocene.

The Karakoram Terrane consists of a pre-Ordovician crystalline basement whose Paleozoic history demonstrates its Gondwana affinity (Gaetani, 1997). Permian to Early Cretaceous sequences indicate a passive margin environment associated with the opening of the Tethys Ocean (Gaetani and Garzanti, 1991). A major, Early to Mid Cretaceous magmatic event produced calc-alkaline plutons (so-called Karakoram Batholith) and mostly andesitic volcanic rocks while the Karakoram had become the active continental margin of southern Asia (e.g. Coward et al., 1986; Debon et al., 1987; Le Fort et al., 1983; Searle et al., 1987). In the studied area, the Karakoram lithologies commonly display a main, suture parallel and steeply NW dipping foliation and SE verging thrusts. Tight to isoclinal folds have axes plunging 25–40°NW. Deformation and metamorphism are generally greenschist facies. However, a wedge of amphibolite-facies gneiss occurs against the KKSZ in the Drosh area (Fig. 1).

The North-Tethys Ocean lithologies are composed of pelagic to hemipelagic sediments, low-grade volcanic rocks (including pillow lavas) and volcano-detritic sediments. Fossilifer-

ous (rudists, orbitolinoids) reef-limestone sequences occur within green basaltic to andesitic volcanites (Pudsey et al., 1985b). It is not clear whether these reef-limestones, tectonically incorporated within the suture zone, were deposited on the Karakoram or Kohistan terranes, or both. Serpentinites occur either as massive lenticular bodies or thin schistose shreds along major faults. The meta-ultramafites mainly occur as talc-magnesite carbonates and schists, indicating circulation of CO_2 fluids within the suture fault system. Like previous authors (Coward et al., 1986; Pudsey et al., 1985a), we could not recognise a typical ophiolitic sequence, a feature also emphasised for the Shyok continuation of the KKSZ (e.g. Rai, 1982; Thakur et al., 1981) and recent reviews (Robertson and Collins, 2002). Also like in the Shyok suture, no blueschist-facies rock has ever been found in the KKSZ.

Rocks display at least three ductile deformation events represented by (1) stretching and mineral lineations in conglomerates and marbles, (2) curved fold axes in greenschists, and (3) crenulation lineations in black schists and slates (Heuberger, 2004). A detailed distinction of the different deformation events remains difficult because of the strong sinistral strike-slip overprint and the lack of precise ages. Indeed, the various rock units are bounded by essentially brittle, anastomosing faults. Slickensides on fault planes indicate brittle, sinistral shear with a minor SE-verging reverse component. In the fault-bounded blocks, the main foliation dips 65–85° towards the Karakoram side and ductile lineations plunge from subhorizontal to 70°SW.

The North Kohistan Arc comprises andesitic volcanic rocks, volcano-detritic and shelf-type sediments, and the calc-alkaline Kohistan Batholith (e.g. Treloar et al., 1996). The main deformation produced the strong, suture-parallel foliation on which the mineral/stretching lineation is subhorizontal (Heuberger, 2004). Volcanogenic greenschists are often crenulated around fold axes parallel to this lineation. Folds in marbles have axes plunging 20–30°NE. Pebbles of fault-bounded, low-grade red conglomerates are elongated in the near down-dip direction, thus defining a stretching lineation transverse to the ductile mineral lineation. This stretching lineation could be evidence for former thrusting. Brittle deformation is principally represented by sinistral strike-slip faulting with a reverse component.

Many studies have shown that a temporal relationship between igneous and metamorphic/structural events typically characterises the tectonic development of suture zones. In order to constrain the history of events that produced the KKSZ, most previous studies of the KKSZ have concentrated on the eastern (Dunlap and Wysoczanski, 2002; Searle et al., 1989) and central Karakoram (Fraser et al., 2001; Rex et al., 1988) and much less on the eastern Hindu Kush (Hildebrand et al., 2001). We focused our efforts on obtaining crystallisation ages of plutonic rocks whose structural setting was carefully characterised along the KKSZ of NW Pakistan (Heuberger, 2004). This paper presents new U-Pb zircon ages, Ar-Ar amphibole and muscovite ages and Hf isotope compositions of

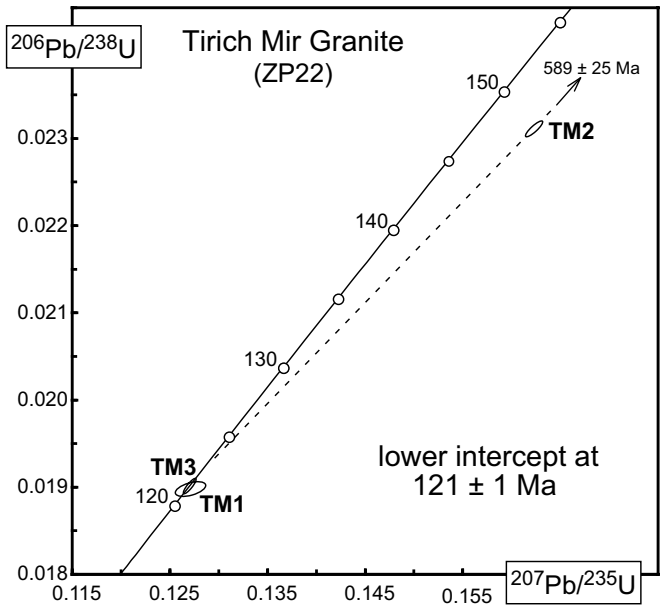

Fig. 2. U-Pb Concordia diagram of the Tirich Mir granite (ZP22). GPS point and analytical data in table 1.

dated zircons from key samples which are important for defining general models of arc-arc collision. We attempt a more detailed interpretation of the Kohistan-Karakoram collision in the NW Himalayas. Methodological information is given in the Appendix.

U-Pb geochronology and initial Hf isotopic composition of zircon

For presentation purposes, we divide our results into the three distinct groupings corresponding to the three main tectonic units described in the geological setting.

Karakoram intrusions

Tirich Mir granite (ZP22)

The Tirich Mir pluton is a weakly deformed but heavily altered two-mica granite that intrudes both the Eastern Hindu Kush and Karakoram magmatic belts and, perhaps more importantly, the metamorphic and ultrabasic rocks of the Tirich Boundary Zone (Zanchi et al., 2000). Stoping and moderate contact metamorphism in host rocks suggest a shallow level of emplacement. Intrusive relationships and dyke swarms are well exposed around the Tirich Mir granite except on its southern margin, where it is thrust on low-grade metamorphic rocks (Zanchi et al., 2000; Hildebrand et al., 2001). A whole-rock Rb-Sr age of 115 ± 4 Ma was reported by (Desio et al., 1964). However, 195 to 188 Ma U-Pb ages of monazites from a deformed leucogranite dyke associated with migmatites docu-

Tab. 1. Results of U-Pb age determinations of Karakoram and suture rocks (**a**) calculated on the basis of radiogenic $^{208}Pb/^{206}Pb$ ratios, assuming concordance; (**b**) corrected for fractionation and spike; (**c**) corrected for fractionation, spike, blank and common lead; (**d**) corrected for initial Th disequilibrium, using an estimated Th/U ratio of 4 for the melt. (*) zircons were not abraded.

			concentrations				atomic ratios										
number	weight (mg)	number of grains	U (ppm)	radiogenic Pb (ppm)	non-radiogenic Pb (pg)	Th/U **(a)**	$^{206}Pb/^{204}Pb$ **(b)**	$^{206}Pb/^{238}U$ **(c,d)**	error 2σ (%)	$^{207}Pb/^{235}U$ **(c)**	error 2σ (%)	$^{207}Pb/^{206}Pb$ **(c,d)**	error 2σ (%)	age **(c,d)** $^{206}Pb/^{238}U$	age **(c,d)** $^{207}Pb/^{235}U$	age **(c,d)** $^{207}Pb/^{206}U$	error corrected
Tirich Mir granite, ZP22, Karakoram, 71°47'40''E/36°11'30''N																	
TM1	0.0010	1	762	14.17	1.1	.28	882	0.01898	0.35	0.12710	0.97	0.04857	0.85	121.2	121.5	127.3	0.50
TM2	0.0040	1	909	21.76	3.5	.40	1521	0.02311	0.32	0.16230	0.43	0.05095	0.21	147.3	152.7	238.4	0.88
TM3	0.0035	1	2281	39.80	1.8	.06	5264	0.01901	0.32	0.12704	0.38	0.04846	0.14	121.4	121.1	121.8	0.88
Phargam granite, 01B04, Karakoram, 72°16'30''E/36°05'07''N																	
1	0.0030	2	757	14.03	0.6	0.84	3878	0.01625	0.35	0.10764	0.45	0.04818	0.25	103.91	104.08	107.96	0.88
2	0.0100	3	719	15.48	1.0	0.16	9934	0.02080	0.35	0.15576	0.39	0.05430	0.16	132.73	146.98	383.54	0.91
3	0.0042	1	55	1.01	1.6	0.94	164	0.01621	0.60	0.10681	4.13	0.04780	3.98	103.64	103.04	89.18	0.32
4	0.0065	2	629	66.91	0.8	0.13	35518	0.10333	0.34	1.34375	0.39	0.09432	0.11	633.9	864.8	1514.5	0.96
5	0.0038	3	442	14.04	0.4	0.22	10649	0.02995	0.65	0.23247	0.66	0.05629	0.48	190.20	212.20	463.90	0.73
6	0.0031	1	587	11.99	1.0	1.23	3072	0.01620	0.63	0.10838	0.86	0.04854	0.65	103.56	104.48	125.50	0.66
Meta-dioritic amphibolite, 01A62, Karakoram, 71°55'48''E/35°44'08''N																	
7	0.0010	2	161	2.83	0.9	0.58	928	0.01646	0.48	0.10963	1.13	0.04830	1.02	105.25	105.63	114.05	0.43
8	0.0050	2	809	13.99	1.1	0.50	3788	0.01648	1.05	0.11066	1.16	0.04869	1.04	105.38	106.57	133.16	0.56
9	0.0042	3	636	11.33	1.7	0.64	1687	0.01644	0.39	0.10965	0.54	0.04836	0.38	105.14	105.64	117.07	0.71
Quartz-diorite, sh2500, Suture, 71°57'25''E/35°43'01''N																	
10	0.0044	2	274	5.32	2.0	0.86	652	0.01677	0.72	0.11263	1.28	0.04879	1.10	107.04	108.37	137.58	0.51
11	0.0020	3	174	3.45	0.9	1.33	439	0.01677	0.78	0.11000	2.30	0.04757	2.12	107.21	105.96	78.04	0.39
12	0.0082	3	287	5.51	1.7	0.87	1497	0.01669	0.45	0.11113	0.70	0.04830	0.55	106.68	107.00	114.10	0.62
Granite dyke, 01A50b, Suture, 71°54'49''E/35°40'13''N																	
13	0.0073	2	449	9.09	9.5	1.09	384	0.01674	0.36	0.11129	1.04	0.04823	0.95	107.00	107.14	110.35	0.41
14	0.0040	3	375	7.48	3.3	1.01	506	0.01678	0.37	0.11160	1.03	0.04823	0.95	107.29	107.45	110.48	0.39
15	0.0009	4	492	10.01	1.0	1.11	4796	0.01672	0.40	1.11130	0.49	0.04828	0.27	106.89	107.16	113.15	0.83
16	0.0113	3	491	10.47	1.7	1.34	3465	0.01671	0.44	0.11080	0.47	0.04809	0.25	106.83	106.69	103.74	0.85
17	0.0030	2	490	10.05	3.4	1.14	481	0.01673	0.40	0.11119	1.09	0.04820	0.98	107.00	107.10	108.90	0.44
Basalt sill, 20.1, Suture, 72°01'20''E/35°46'22''N																	
18*	0.0032	1	119	1.96	0.3	0.13	1158	0.01673	0.80	0.11718	1.41	0.05078	1.27	107.00	112.50	230.99	0.45
19*	0.0020	2	196	3.87	1.4	0.93	466	0.01672	0.63	0.11260	1.42	0.04883	1.30	106.92	108.34	108.34	0.40
20*	0.0082	5	801	15.29	0.9	0.85	2945	0.01664	0.46	0.11108	0.54	0.04840	0.39	106.40	106.95	118.99	0.71

Fig. 3. Field view of the Phargam granite (01B04): Dioritic enclaves and magmatic minerals show no sign of plastic deformation. (GPS: N 36°04'40.8"; E 72°14'29.4").

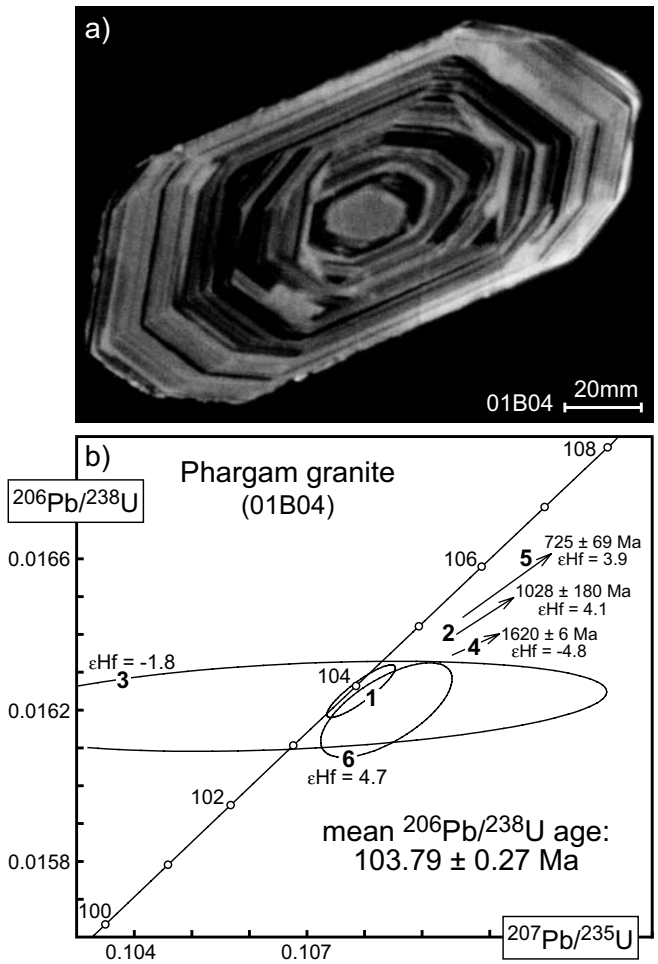

Fig. 4. Zircons of the 01B04 Phargam granite; a) Cathodoluminescence image of a representative zircon; b) U-Pb Concordia diagram. GPS point and analytical data in table 1.

ment early Jurassic magmatism and metamorphism whereas monazites and uraninites from a pegmatite dyke on the west side of the Tirich Mir granite are dated between 125 and 112 Ma (Hildebrand et al., 2001). In order to constrain the suturing age of the Tirich Boundary Zone, it was therefore essential to have a precise intrusion age of this granite.

A. Zanchi collected the sample chosen for new radiometric dating (ZP22), a loose block at the foot of a big rock wall in the upper part of the Dir Gol, along the western side of the Tirich Mir intrusion. The sample contained red-to-brown euhedral zircons. Three grains with variable U concentrations between 762 and 2281 ppm (Table 1) resulted in two concordant and one discordant point (Fig. 2). A best-fit line yields an upper intercept age of 589 ± 25 Ma and a lower intercept of 121 ± 1 Ma. The latter, through the concordant points, is interpreted as the age of emplacement.

Phargam granite (01B04)

A coarse-grained, porphyritic alkali-granite occurs in the area of the Phargam An, intrusive into low-grade slates, quartzites, volcanosedimentary sequences, marbles and calcareous conglomerates. It forms an isolated pluton, about 10 km in diameter, located 3–5 km to the northwest of the KKSZ. This granite crosscuts the deformation structures of the country rocks (Fig. 3).

The dated sample was collected northeast of the Phargam An, the Pass connecting the Golen with Phargam Gol. It displays a magmatic, porphyric texture but no sign of plastic deformation. Magmatic minerals are K-feldspar, plagioclase, quartz, biotite ± titanite. Accessory minerals are zircon, apatite and unspecified ores. Alteration products are muscovite, chlorite and epidote. Cathodoluminescence (CL) images of zircons reveal undisturbed oscillatory zoning patterns (Fig. 4a).

Tab. 2. Results of Hf isotopic determinations of dated zircon microfractions from Karakoram, suture and Kohistan units. N.D. = Not detected; t = time (**a**) measured $^{176}Hf/^{177}Hf$; (**b**) numbers refer to the last digits; (**c**) corrected for fractionation, normalised to JMC standard 0.282160; (**d**) as (c) and age corrected with $^{176}Lu/^{177}Hf$=0.005.

number	$^{176}Hf/^{177}Hf$ measured (a)	±2σ % (b)	$^{176}Hf/^{177}Hf$ normalised (c)	$^{176}Hf/^{177}Hf$ (t) (d)	$\varepsilon Hf^{(t)}$
Phargam granite, 01B04, Karakoram					
1	N.D.	N.D.	N.D.	N.D.	
2	0.282814	7	0.282803	0.282790	4.1
3	0.282671	30	0.282655	0.282645	-1.8
4	0.282241	5	0.282225	0.282163	-4.8
5	0.282775	9	0.282759	0.282741	3.9
6	0.282854	9	0.282838	0.282828	4.7
Meta-dioritic amphibolite, 01A62, Karakoram					
7	0.282824	23	0.282808	0.282798	3.7
8	0.282740	10	0.282768	0.282758	2.3
9	0.282771	11	0.282799	0.282789	3.4
Quartz-diorite, sh2500, Suture					
10	0.282918	6	0.282946	0.282935	8.6
11	0.282861	24	0.282889	0.282878	6.6
12	0.282921	4	0.282949	0.282939	8.7
Granite dyke, 01A50b, Suture					
13	0.283017	8	0.283011	0.283001	10.9
14	0.282937	9	0.282931	0.282921	8.1
15	0.282930	14	0.282919	0.282909	7.6
16	0.282963	10	0.282952	0.282942	8.8
17	N.D.	N.D.	N.D.	N.D.	
Basalt sill, 20.1, Suture					
18	N.D.	N.D.	N.D.	N.D.	
19	0.282976	12	0.283004	0.282993	10.6
20	0.282951	11	0.282979	0.282969	9.8
Mirkhani diorite, 01B25, Kohistan					
21	0.283085	7	0.283113	0.283102	14.6
22	0.283072	10	0.283100	0.283089	14.2
23	N.D.	N.D.	N.D.	N.D.	
24	0.283058	14	0.283086	0.283075	13.7
25	N.D.	N.D.	N.D.	N.D.	
Meta-gabbro, 01B24, Kohistan					
26	0.283082	3	0.283076	0.283072	11.8
27	0.283093	2	0.283087	0.283083	12.2
28	0.283087	4	0.283076	0.283071	11.9
29	0.283052	4	0.283041	0.283037	10.6
Granite dyke, 01B22, Kohistan					
30	0.282589	3	0.282583	0.282578	-5.6
31	0.282520	5	0.282514	0.282495	-4.7
32	0.282635	3	0.282629	0.282610	-0.5
33	0.282772	5	0.282761	0.282749	2.5
34	0.282721	6	0.282710	0.282694	1.7
35	0.282558	5	0.282586	0.282570	-2.8
36	N.D.	N.D.	N.D.	N.D.	
37	0.282666	5	0.282694	0.282690	-1.6
Granite dyke, 01A07, Kohistan					
38	0.282968	7	0.283062	0.283059	11.2
39	0.282950	11	0.283044	0.283040	10.5
40	0.282953	13	0.282981	0.282977	8.3
41	0.282967	10	0.282995	0.282991	8.8
42	0.282877	5	0.282905	0.282900	5.8

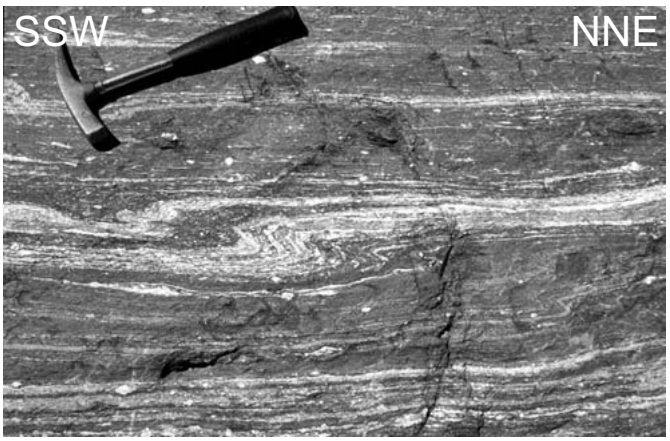

Fig. 5. Field view of meta-dioritic amphibolite (01A62): The mylonitic foliation is deformed by drag folds consistently showing sinistral shear (top to SSW, foliation dipping >45°NNW). (GPS: N 35°33'48.8"; E 71°46'02.1").

Four microfractions and two single grains were analysed (Table 1, Fig. 4b). Zircon microfractions 1, 3 and 6 have yielded $^{206}Pb/^{238}U$ ages between 103.5 and 104.0 Ma. Analyses 1 and 3 are concordant whereas microfraction 6 is subconcordant and displays slightly higher $^{207}Pb/^{235}U$ ratios probably due to inheritance. Analysis number 3 represents a single zircon with low U (55 ppm) and radiogenic Pb (1.01 ppm) concentrations, resulting in an enhanced $^{207}Pb/^{235}U$ uncertainty. These ages date magmatic growth of zircons as the grains show characteristic oscillatory zoning (Fig. 4a). Microfractions 2, 4 and 5 yielded $^{206}Pb/^{238}U$ ages between 132 and 634 Ma and were used to estimate the age of inherited components by regressing the discordant analyses together with the (near-) concordant points 1, 3 and 6. Upper intercepts indicate source ages of (725 ± 39 Ma; analysis 5), (1028 ± 180 Ma; analysis 2), and (1620 ± 6 Ma; analysis 4). These ages are attributed to small inherited cores within the 104 Ma zircons, which have not been detected during CL imaging. The mean $^{206}Pb/^{238}U$ age calculated from zircon analyses 1, 3 and 6 is 103.79 ± 0.27 Ma and is interpreted as intrusion age of the Phargam granite.

The zircons of this sample yielded widely scattered εHf values (Table 2). The concordant analyses 3 and 6 have εHf of -1.8 and +4.7. The discordant points 2, 4 and 5 do not show correlation between the εHf values and the different degrees of inheritance, suggesting that the polyphase zircons had different sources and/or contain cores with already different phases.

Meta-dioritic amphibolite (01A62)

The Karakoram plate hosts a 75 km long unit of sheared gabbros and dioritic rocks (Fig. 5), which also includes minor quartzo-feldspathic migmatites, meta-granitic dykes and hornblendites. The gabbros and diorites intruded volcano-sedimentary sequences and display southeastwards increasing strain, towards the suture. This strain gradient is related to suturing and/or post-suturing deformation between Kohistan and Kara-

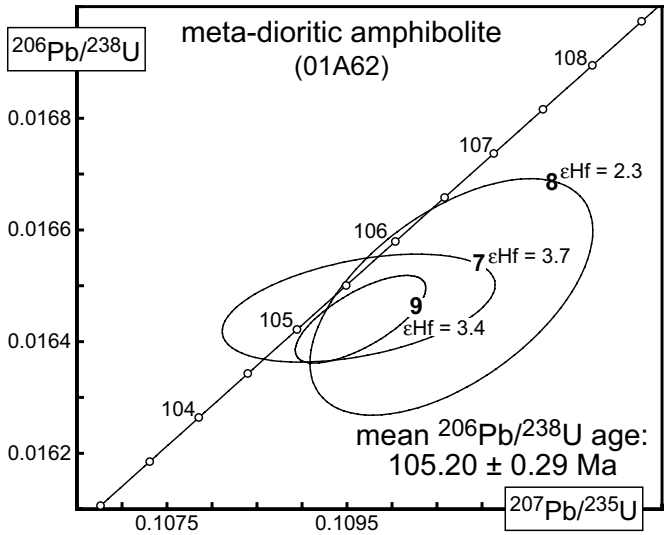

Fig. 6. U-Pb Concordia diagram of the meta-dioritic amphibolite (01A62). GPS point and analytical data in table 1.

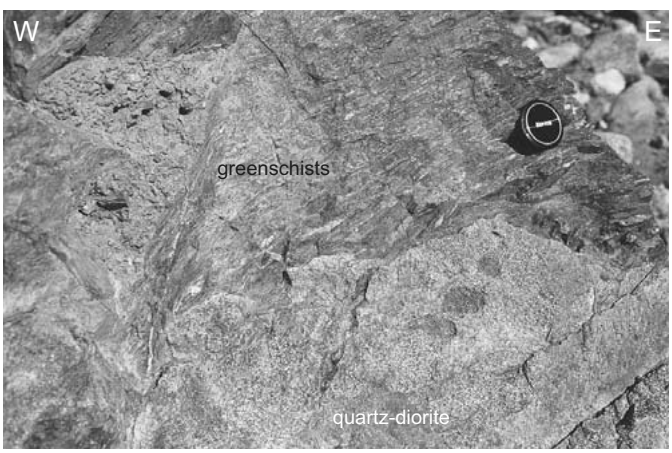

Fig. 7. Intrusive contact of the quartz-diorite (sh2500) into foliated (060-56NW) volcanoclastic greenschists of the KKSZ at N 35°43' 6.2"; E 71°57' 27.3".

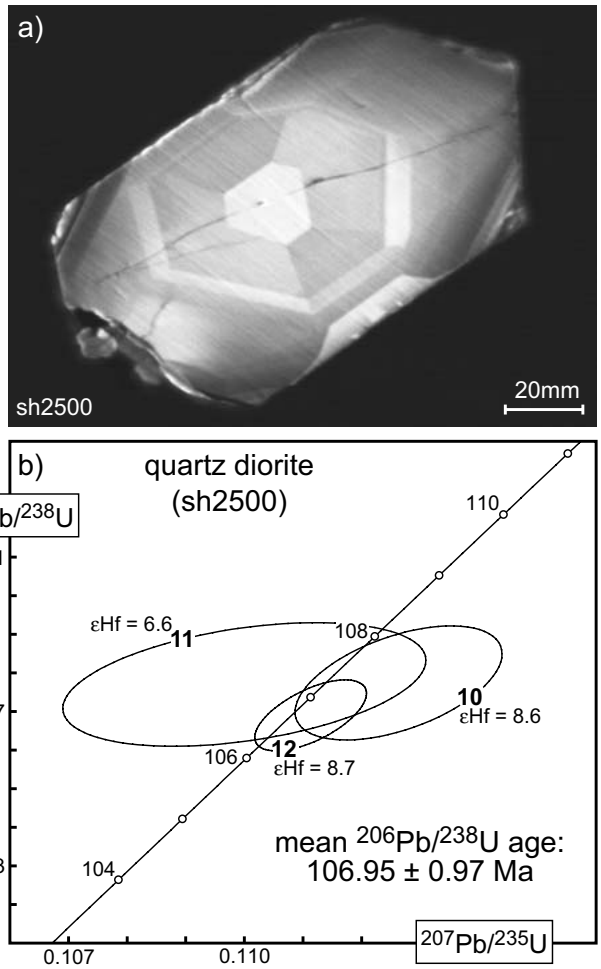

Fig. 8. Zircons of the quartz-diorite (sh2500); a) Cathodoluminescence image of a representative, non-abraded zircon; b) U-Pb Concordia diagram. GPS point and analytical data in table 1.

koram (Heuberger, 2004). Therefore, the intrusion age of the dated meta-dioritic amphibolite sets a maximum age of that deformation phase(s).

The sample was taken from the southeasternmost outcrop of this rock unit in the Kalas Gol, 1.5 km northwest of the suture zone. The rock is strongly foliated, but the magmatic texture is locally preserved. Magmatic minerals are magnesio-hornblende, feldspar, biotite, titanite, ilmenite ± quartz. The metamorphic paragenesis is made of recrystallised plagioclase, hornblende, epidote, chlorite, actinolite ± garnet. Accessory minerals are brown spinel, zircon and apatite.

The 0.7 kg sample yielded 25 small euhedral zircons containing tiny melt inclusions, presumably of magmatic origin. Three zircon microfractions (7, 8 and 9) containing 2 to 3 grains were analysed (Table 1, Fig. 6). The $^{206}Pb/^{238}U$ ages range between 105.1 and 105.4 Ma and define a precise intrusion age of 105.20 ± 0.29 Ma (Fig. 6). The three zircon microfractions yielded a mean εHf value of +3.0 ± 1.6 (Table 2).

Intrusions within the suture

The KKSZ in the Chitral area includes tectonically imbricated units of different origin. However, a general polarity can be identified across the suture zone, from NW to SE: (1) calc-alkaline plutons and shallow-water sediments intercalated with andesitic volcanic rocks of the Karakoram terrane, (2) marine sediments, volcanic rocks with local pillow lavas and meta-ultramafic rocks attributed to the North-Tethys oceanic basin and (3) basalts and andesites interlayered with Aptian-Albian fossiliferous limestones; this association lays over turbiditic red shales, sandstones and conglomerates attributed to the Kohistan Arc, along with the volcanogenic greenschists, metabasaltic amphibolites and meta-gabbros found further to the south.

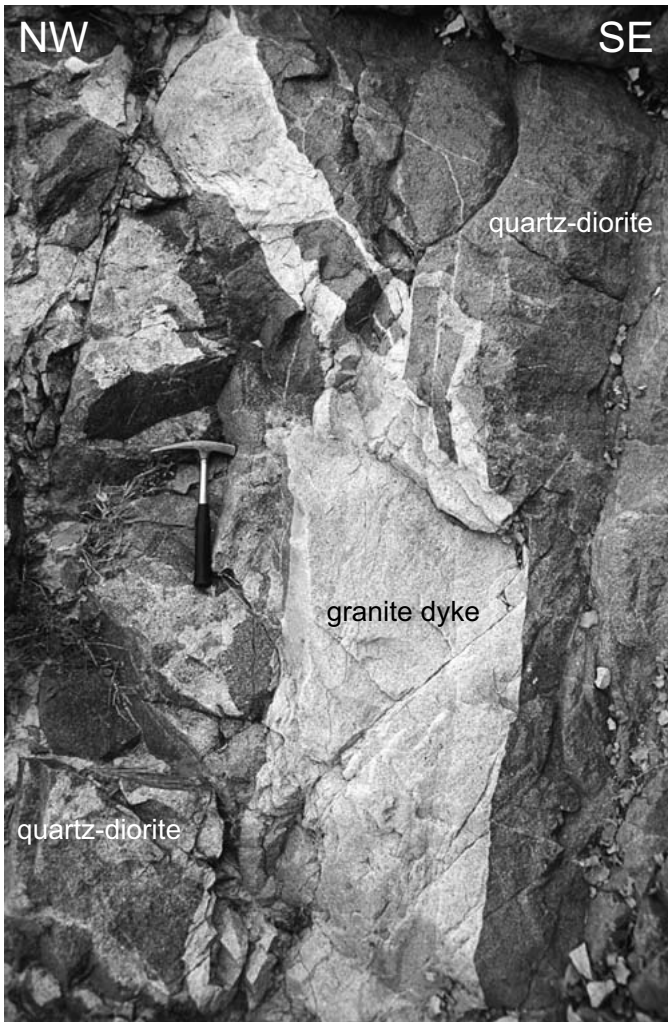

Fig. 9. Granite dyke (01A50b) intruding a quartz-diorite at the sample location. GPS point and analytical data in table 1

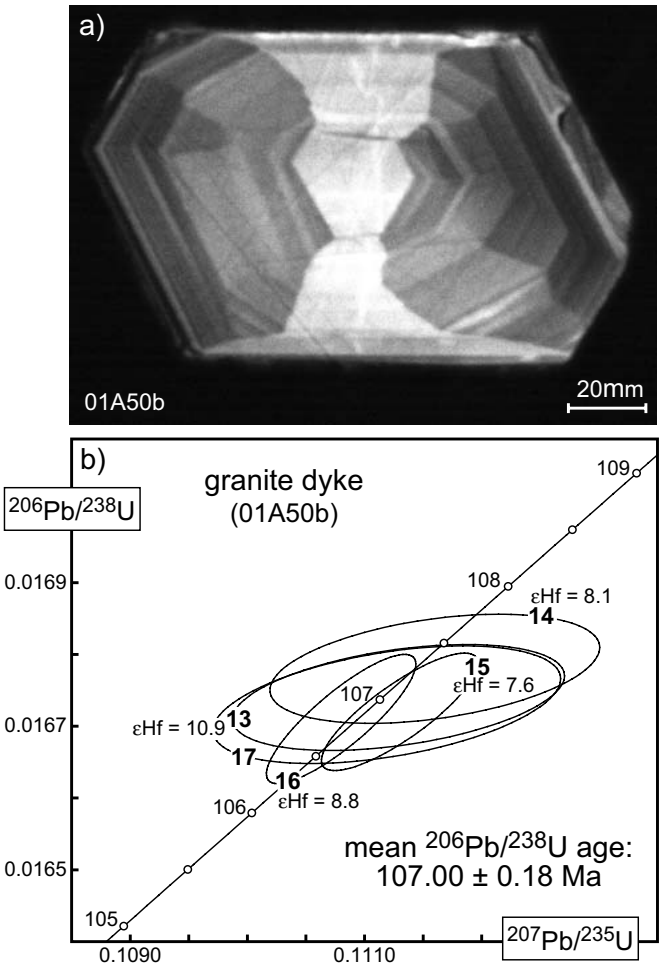

Fig. 10. Zircons of the granite dyke (01A50b); a) Cathodoluminescence image and b) U-Pb Concordia diagram. GPS point and analytical data in table 1.

Quartz-diorite (sh2500)

This quartz-diorite has intruded volcanoclastic and calcareous sequences and is faulted against serpentinites and talcschists along its northern boundary (Fig. 7). Flattened mafic xenoliths and subvertical hornblende crystals define the weak, probably magmatic fabric of this medium-grained rock. Magmatic minerals are plagioclase, hornblende, quartz, biotite and titanite. Alteration products are muscovite, epidote ± chlorite.

The sample was taken 500 m upstream in the Domuk Gol. CL images of zircons display undisturbed growth textures with dominant sector zoning, typical for mafic magmatic rocks (Fig. 8a). Three zircon microfractions containing 2 to 3 grains were analysed (Table 1, Fig. 8b) with $^{206}Pb/^{238}U$ ages ranging between 106.7 and 107.2 Ma. The scatter in ^{207}Pb is considered to be an artefact of common lead correction. The average $^{206}Pb/^{238}U$ age of 106.95 ± 0.97 Ma is interpreted to date the intrusion of this quartz-diorite. The zircons yield a mean εHf value of +8.2 ± 2.5 (Table 2).

Granite dyke (01A50b)

A quartz-diorite pertaining to the gabbros and diorites within the suture was intruded by a granite dyke, 1.5 km north of Gawuch. The host quartz-diorite intruded calcareous turbidites represented today as a thrust wedge of hornfelses within serpentinite and talcschists (Fig. 9). The granite was sampled 1.7 km N of the village Gawuch, 350 m to the NW above the Shishi Gol jeep road. The magmatic assemblage consists of quartz, hornblende, plagioclase ± pyroxene ± biotite and opaque minerals. Plagioclase is strongly altered to muscovite and chlorite. Zircon exhibits undisturbed oscillatory patterns, with local sector zoning (Fig. 10a) indicating a magmatic origin. Five zircon microfractions with 2 to 4 zircons were analysed (Table 1), which form a coherent cluster with a mean $^{206}Pb/^{238}U$ age of 107.00 ± 0.18 Ma. This age is interpreted as the crystallisation of zircon during dyke emplacement. The εHf values scatter between +7.6 and +10.9, with a mean value of +8.9 ± 2.3 (Table 2).

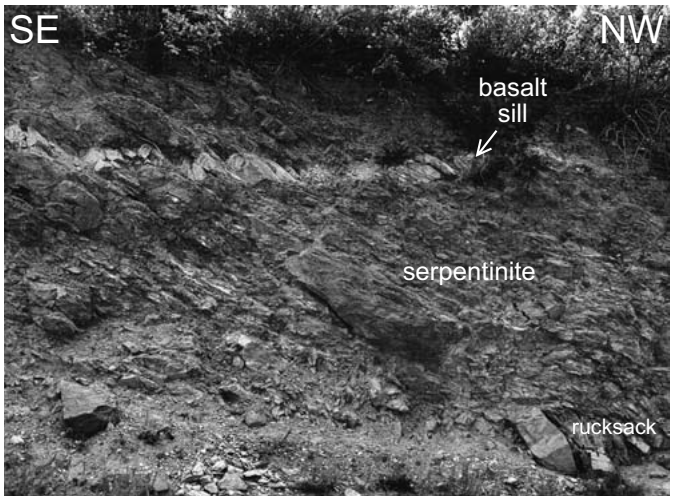

Fig. 11. Subhorizontal basalt sill (20.1) crosscutting the NW-dipping foliation of serpentinite at the sampling site, GPS: N 35°46'22"; E 72°01'20".

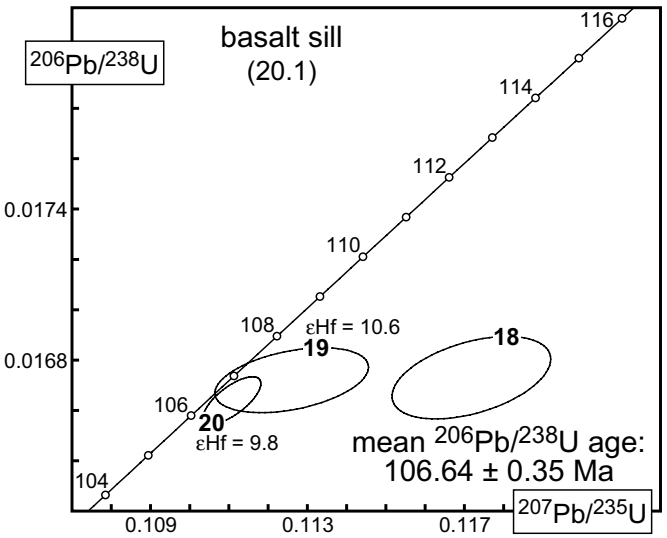

Fig. 12. U-Pb Concordia diagram from zircons of the basalt sill (20.1). GPS point and analytical data in table 1.

Basalt sill (20.1)

An undeformed, yet altered basalt sill crosscuts imbricate serpentinites and talc schists in the Chhuchhu Gol, about 1 km to the SW of Madaglasht (Fig. 11). It therefore yields a minimum age for the meta-harzburgite serpentinisation and deformation. Outcrops were insufficiently clear to ascertain whether this sill also crosscuts faults separating the serpentinite from other suture units, and thus whether the sill also gives an age constraint on the suturing-related brittle imbrication.

The 0.85 kg sample was taken at the entrance of the Chhuchhu Gol just N of the Shishi Gol jeep road. The magmatic paragenesis is represented by brown ± green amphibole, titanite and hematite. Greenschist-facies alteration products are calcite, chlorite, epidote, muscovite, albite and actinolite. Accessory minerals are zircon, apatite and opaque minerals. The sample yielded 12 zircons, nine of which were grouped into three analytical fractions containing 1 to 5 zircons. The three remaining zircons were not used because they were broken and had a brown colour, suggesting that they are metamict and therefore likely to have suffered Pb loss, or contained inclusions. The zircons were not abraded and not prepared for cathodoluminescence imaging to avoid loss of material during the procedure. We assume the zircons to be magmatic because there is no high-grade (>amphibolite facies), post-crystallisation metamorphic event recorded in the mineral paragenesis. Rim recrystallisation due to greenschist-facies fluid alteration cannot be ruled out.

The three analyses plot slightly to moderately to the right of the concordia line (Table 1, Fig. 12). The $^{207}Pb/^{235}U$ ratio is inversely correlated to the U concentration, in agreement with a constant ^{207}Pb excess component being present in the zircons. The mean $^{206}Pb/^{238}U$ age of 106.64 ± 0.35 Ma is interpreted as intrusion age of the sill. The two concordant fractions yield a mean εHf of +10.2 ± 0.6 (Table 2).

Fig. 13. The Mirkhani diorite (01B25) at the sampling site (GPS in table 1). Note the magmatic fabric and undeformed xenoliths.

Kohistan intrusions

On the Kohistan side of the suture, the steeply NW-dipping lithologies of the Kohistan Paleo-Island Arc Complex, such as mylonitic gabbros and amphibolites, former volcanoclastic sediments and lavas are crosscut by variously foliated dykes and leucogranites, which will be used to constrain young arc-related magmatism and deformation.

Mirkhani diorite (01B25)

This diorite (Fig. 13) has intruded basaltic to andesitic lavas and shallow water, Aptian (125-112 Ma; Stratigraphy, 2004) fossiliferous limestones. It is faulted against greenschists and marbles about 10 km to the SW of Drosh. The sample was taken on the Chitral-Lowari Pass road, 1 km SW of the

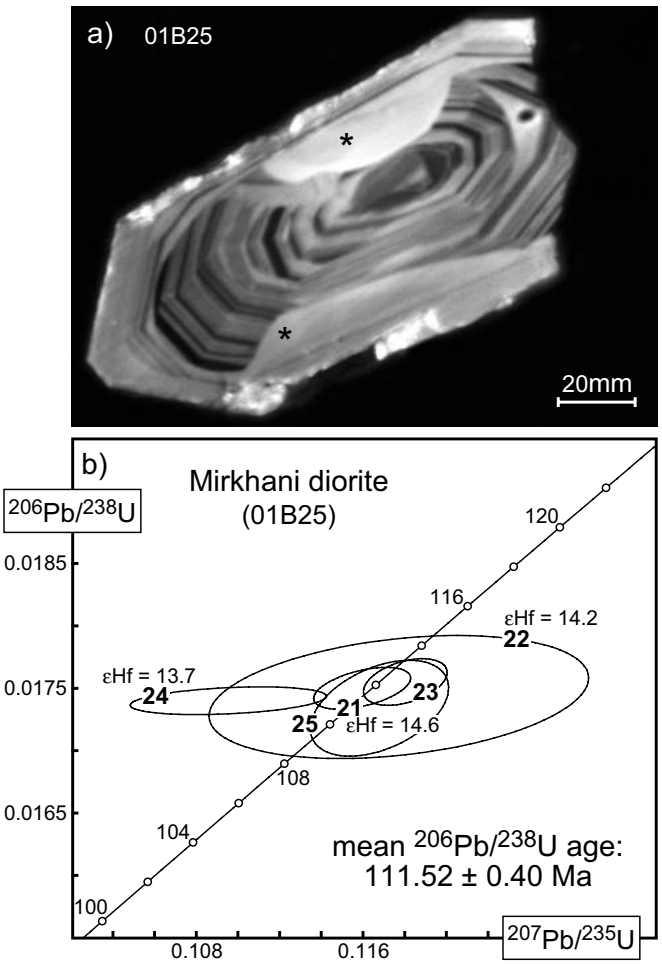

Fig. 14. Zircons of the Mirkhani diorite (01B25); a) Cathodoluminescence image; asterisks marks homogeneous domains interpreted as recrystallised; b) U-Pb Concordia diagram. GPS point and analytical data in table 3.

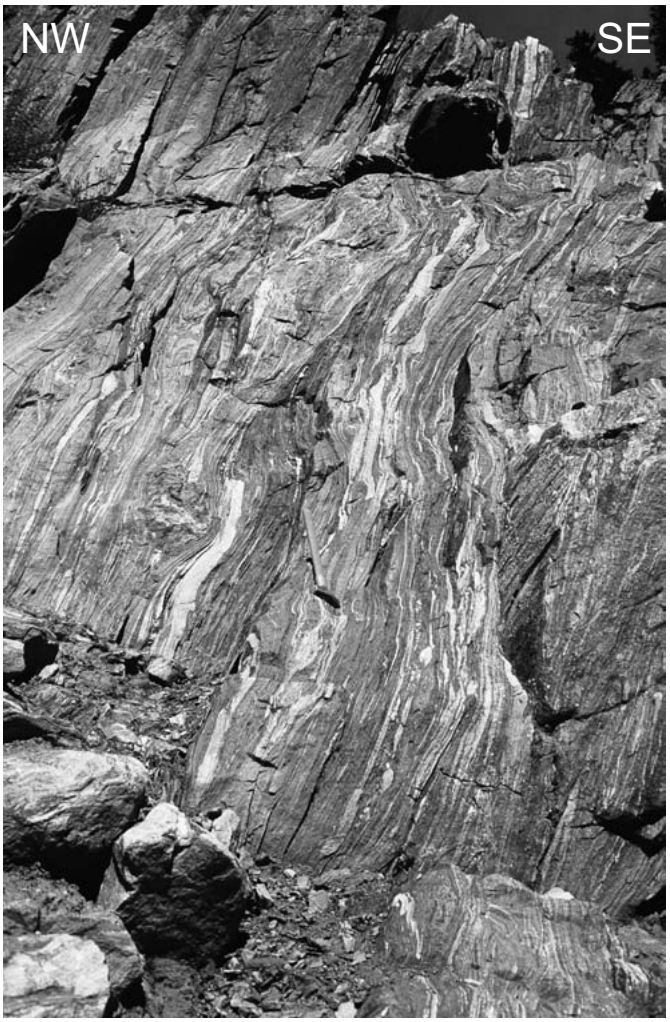

Fig. 15. Field view of the strongly foliated meta-gabbro (01B24) at its sampling point (GPS in table 3). Note the characteristically steep foliation.

Mirkhani junction. Plagioclase, K-feldspar, quartz, hornblende ± titanite are magmatic minerals. Epidote, biotite and chlorite are retrograde minerals. Cathodoluminescence images of euhedral zircons show undisturbed oscillatory zoning patterns (Fig. 14a) indicating that zircons are magmatic. Homogeneous prism zones (stars on Fig. 14a) may represent recrystallised domains. The relatively high degree of alteration of the sample is consistent with the slightly corroded zircon rims.

Four out of five zircon analyses are concordant whereas one (analysis 24) is inversely discordant, considered to be an artefact of the poor accuracy of measured $^{206}Pb/^{204}Pb$ ratios (Table 3, Fig. 14b). The five analyses yielded a mean $^{206}Pb/^{238}U$ age of 111.52 ± 0.40 Ma, interpreted as intrusion age of the diorite, and consistent with the older, Aptian (125-112 Ma) age of the host volcanic rocks and limestones. The εHf values scatter between +13.7 and +14.6, with a mean value of +14.3 ± 1.1 (Table 2).

Meta-gabbro (01B24)

Meta-gabbros and -diorites are intrusive in mafic volcanic and volcanoclastic rocks. They are strongly deformed into locally ultramylonitic shear zones (Fig. 15).

The weakly foliated, amphibolite-facies 01B24 meta-gabbro was sampled 17 km south of Drosh on the Chitral-Lowari Pass road. It contains magmatic tschermakite, biotite, plagioclase, ilmenite, titanite ± pyroxene. The metamorphic paragenesis is represented by plagioclase, biotite ± garnet ± actinolite ± chlorite ± epidote. Zircons show either a faint, oscillatory zoning on cathodoluminescence images (Fig. 16a) or sector zoning in the center combined with planar, oscillatory zoning along the rims (Fig. 16b). The textures indicate that zircons are magmatic. Thin and discordant high luminescence rims (which were removed by abrasion prior to analysis) represent discordant overgrowth that may reflect recrystallisation or growth of new zircon during the post-magmatic, metamorphic event.

Tab. 3. Results of U-Pb age determinations of Kohistan rocks. Same keys as Table 1.

			concentrations				atomic ratios										
number	weight (mg)	number of grains	U (ppm)	radiogenic Pb (ppm)	non-radiogenic Pb (pg)	Th/U **(a)**	$^{206}Pb/^{204}Pb$ **(b)**	$^{206}Pb/^{238}U$ **(c,d)**	error 2σ (%)	$^{207}Pb/^{235}U$ **(c)**	error 2σ (%)	$^{207}Pb/^{206}Pb$ **(c,d)**	error 2σ (%)	age **(c,d)** $^{206}Pb/^{238}U$	age **(c,d)** $^{207}Pb/^{235}U$	age **(c,d)** $^{207}Pb/^{206}U$	error corrected
Mirkhani diorite, 01B25, Kohistan, 71°44'06"E/35°27'54"N																	
21	0.0017	1	384	7.43	1.1	0.77	699	0.01750	0.78	0.11596	1.64	0.04807	1.43	111.82	111.40	102.52	0.49
22	0.0019	2	135	2.54	0.5	0.59	574	0.01743	2.31	0.11772	6.32	0.04899	6.03	111.39	113.01	147.28	0.31
23	0.0036	3	162	3.10	0.4	0.64	1669	0.01755	0.87	0.11803	1.39	0.04877	1.30	112.17	113.28	136.73	0.41
24	0.0012	3	291	5.48	3.1	0.64	143	0.01740	0.52	0.10954	3.51	0.04566	3.38	111.20	105.54	103.74	0.41
25	0.0026	2	338	6.19	4.0	0.52	258	0.01734	1.81	0.11679	2.32	0.04885	2.24	110.82	112.16	140.62	0.43
Meta-gabbro, 01B24, Kohistan, 71°46'01"E/35°24'25"N																	
26	0.0652	3	512	3.41	2.7	0.24	5356	0.00688	0.34	0.04454	0.41	0.04697	0.17	44.18	44.24	47.28	0.91
27	0.0398	4	430	2.94	1.5	0.24	5227	0.00706	0.42	0.04581	0.45	0.04706	0.26	45.36	45.48	52.03	0.82
28	0.0166	5	251	1.97	0.6	0.35	3538	0.00778	0.61	0.05065	0.67	0.04736	0.59	49.80	50.17	67.64	0.58
29	0.0170	3	640	4.56	0.7	0.31	7042	0.00714	0.34	0.04657	0.40	0.04727	0.21	45.89	46.21	62.88	0.85
Granite dyke, 01B22, Kohistan, 71°47'29"E/35°29'09"N																	
30	0.0382	3	936	7.46	2.3	0.52	7331	0.00750	0.35	0.04893	0.40	0.04734	0.15	48.15	48.50	66.25	0.93
31	0.0202	5	196	5.65	0.5	0.06	14751	0.03024	0.34	0.23850	0.38	0.05721	0.13	192.00	217.20	499.70	0.94
32	0.0153	4	626	19.42	1.8	0.31	10398	0.03121	0.35	0.22110	0.39	0.05138	0.14	198.10	202.80	257.80	0.93
33	0.0120	3	414	7.79	0.6	0.11	9770	0.01962	0.35	0.13715	0.40	0.05071	0.16	125.20	130.50	227.40	0.92
34	0.0150	3	372	10.04	1.5	0.36	6251	0.02265	0.33	0.18757	0.40	0.05127	0.16	168.80	174.60	253.10	0.92
35	0.0063	4	621	15.70	0.6	0.13	10835	0.02570	0.47	0.19021	0.48	0.05537	0.30	163.61	176.80	357.20	0.80
36	0.0139	4	1094	10.76	0.7	0.15	13478	0.00940	0.61	0.06490	0.60	0.05007	0.37	60.32	63.90	198.20	0.81
37	0.0062	2	557	4.48	0.3	0.23	4994	0.00774	0.59	0.05123	0.59	0.04802	0.49	49.69	50.70	99.60	0.66
Granitic dyke, 01A07, Kohistan, 71°47'51"E/35°28'31"N																	
38	0.0059	2	339	2.32	1.9	0.36	423	0.00600	1.09	0.03944	2.72	0.04477	2.59	38.55	39.28	83.99	0.32
39	0.0056	2	689	4.66	0.5	058	3025	0.00623	0.81	0.04048	0.71	0.04716	0.61	40.01	40.30	57.21	0.69
40	0.0034	3	369	2.49	1.0	1.89	515	0.00603	0.67	0.03847	2.11	0.04628	2.00	38.74	38.33	12.40	0.32
41	0.0030	3	737	5.03	0.7	0.39	1198	0.00607	1.13	0.03969	1.52	0.04747	1.42	38.98	39.53	72.70	0.46
42	0.0053	4	591	4.72	0.9	0.22	1776	0.00763	0.66	0.05075	0.79	0.04825	0.74	49.00	50.27	111.34	0.49

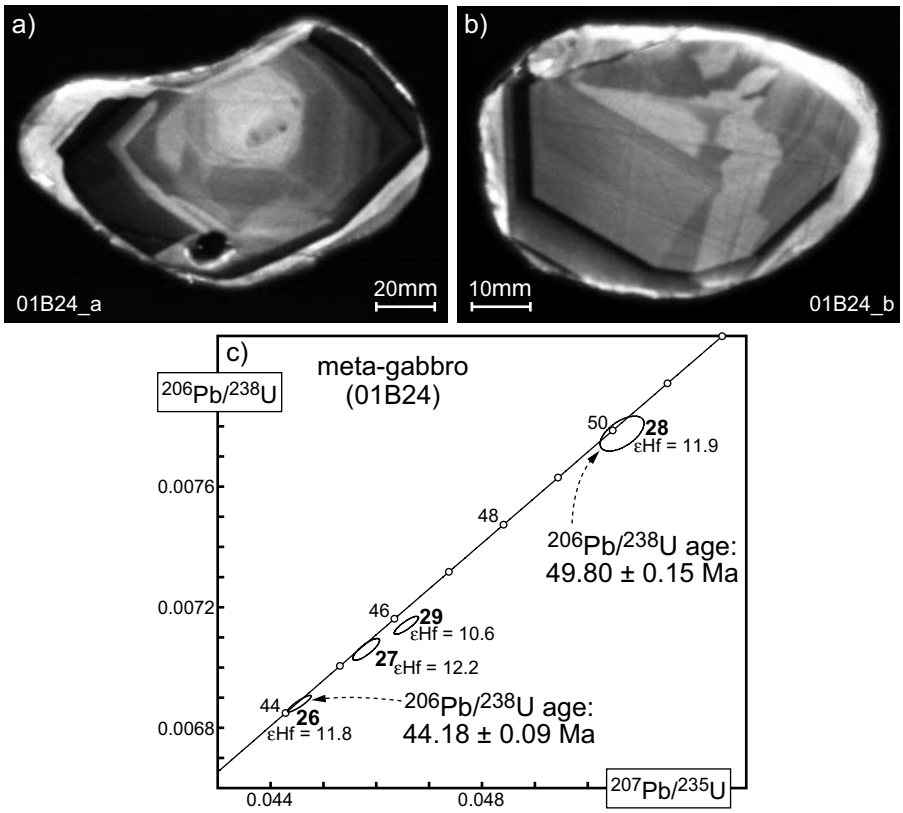

Fig. 16. Zircons of the meta-gabbro (01B24); a) and b) cathodoluminescence images of representative, non-abraded zircons; c) U-Pb Concordia diagram. GPS point and analytical data in table 3.

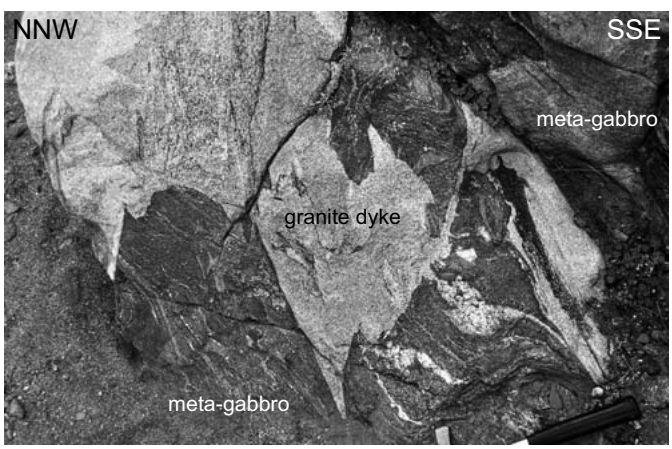

Fig. 17. Granite dyke (01B22) folded and foliated in accordance with the meta-gabbros and -diorites of the Kohistan Arc in which it has intruded. Sampling location, GPS in table 3.

Four zircon microfractions of 3 to 5 grains were analysed (Table 3, Fig. 16c). Analyses 26 and 28 are concordant at $^{206}Pb/^{238}U$ ages of 44.18 ± 0.09 and 49.80 ± 0.15 Ma, respectively. Analyses 26, 27 and 29 define a discordia line with a lower intercept age of 44.1 ± 8.2 Ma and an upper intercept age of ca. 409 Ma. The intrusion age of this meta-gabbro is inferred from the concordant fraction at 49.80 ± 0.15 Ma ($^{206}Pb/^{238}U$ age). The youngest age is tentatively interpreted as a postcrystallisation metamorphic event at 44.18 ± 0.09 Ma ($^{206}Pb/^{238}U$). The two ages of analyses 27 and 29 between the concordant points are interpreted as mixing ages of the magmatic, 49.8 Ma zircons with younger, 44.2 Ma metamorphic overgrowths, possibly combined with some degree of inheritance of Paleozoic age. The Hf isotopic composition of the dated zircons does not reflect the disturbance of the U-Pb system: All four analyses yield εHf values between +10.5 and +12.1, with a mean of +11.6 ± 1.1 (Table 2).

Granite dyke (01B22)

The sampled granite dyke is folded and foliated like and in accordance with the meta-gabbros and -diorites of the Kohistan Arc into which it has intruded (Fig. 17). It was collected on the Beorai Gol jeep road 8 km south of Drosh. Magmatic minerals are quartz, K-feldspar, plagioclase and biotite; the metamorphic paragenesis is represented by chlorite ± garnet ± muscovite. Zircons show polyphase growth, replacement and recrystallisation textures on cathodoluminescence images (Fig. 18a) along with inherited zircon cores (Fig. 18b, arrow).

The eight analysed zircon microfractions of 2 to 5 grains each are discordant (Table 3, Fig. 18c) and yielded $^{206}Pb/^{238}U$ ages between 48 and 198 Ma. They were used to calculate a series of upper intercept ages, ranging from 273 to 871 Ma. The two youngest microfractions (30 and 37) define a discordia line with a lower intercept at 47.4 ± 0.5 Ma, which is regarded as

Tab. 4. Ar-Ar stepwise heating results. All Ar concentrations are in picolitres per gram (pl g^{-1}). Errors are 1σ. Ar* denotes total ^{40}Ar minus atmospheric ^{40}Ar. The integrated K_2O and CaO values are given in weight%. Cl is given in ppm. These values are calculated from the total interference-corrected ^{39}Ar, ^{38}Ar and ^{37}Ar, the production ratios and the irradiation time.

Step	T (°C)	$^{40}Ar_{tot}$	^{39}Ar	^{38}Ar	^{37}Ar	^{36}Ar	Age ± 1σ Ma
20.1 (22.2 mg; J = 3.65*10-3; Ar* = 1905; K20 = 0.56; CaO = 7.4; Cl = 87)							
1	652	37.15 ± 0.01	0.367 ± 0.016	0.087 ± 0.014	1.26 ± 0.06	0.146 ± 0.011	0.0 ± 62
2	856	172.55 ± 0.00	2.834 ± 0.015	0.481 ± 0.021	5.31 ± 0.06	0.441 ± 0.008	96.5 ± 5.4
3	901	36.12 ± 0.15	0.731 ± 0.012	0.041 ± 0.018	2.32 ± 0.06	0.088 ± 0.015	89.8 ± 38
4	942	38.41 ± 0.04	0.662 ± 0.024	0.109 ± 0.022	4.53 ± 0.17	0.112 ± 0.009	54.8 ± 26
5	982	48.22 ± 0.06	1.017 ± 0.009	0.163 ± 0.020	8.00 ± 0.10	0.091 ± 0.007	136.8 ± 13
6	1001	87.98 ± 0.02	3.289 ± 0.018	0.414 ± 0.014	19.84 ± 0.13	0.125 ± 0.013	102.5 ± 7.1
7	1021	137.43 ± 0.14	6.085 ± 0.021	0.858 ± 0.011	37.40 ± 0.18	0.109 ± 0.013	113.7 ± 3.7
8	1040	81.23 ± 0.01	3.295 ± 0.014	0.436 ± 0.010	20.11 ± 0.11	0.055 ± 0.009	128.7 ± 4.7
9	1057	104.98 ± 0.10	4.547 ± 0.013	0.488 ± 0.020	27.51 ± 0.12	0.171 ± 0.009	80.4 ± 3.7
10	1077	404.05 ± 0.03	21.362 ± 0.026	2.407 ± 0.016	124.78 ± 0.36	0.170 ± 0.011	109.1 ± 0.8
11	1095	779.27 ± 0.18	42.593 ± 0.040	4.874 ± 0.018	252.99 ± 0.72	0.318 ± 0.012	106.2 ± 0.4
12	1125	132.06 ± 0.00	5.921 ± 0.015	0.749 ± 0.018	35.27 ± 0.14	0.139 ± 0.011	101.7 ± 3.4
13	1160	68.81 ± 0.04	2.658 ± 0.019	0.286 ± 0.014	15.34 ± 0.13	0.075 ± 0.014	115.1 ± 9.1
14	1490	460.86 ± 0.08	22.249 ± 0.02	2.806 ± 0.014	135.28 ± 0.40	0.276 ± 0.011	112.2 ± 0.8
01B16 (30.0 mg; J = 0.805*10-3; Ar* = 787; K20 = 1.69; CaO =18.6; Cl = 383); 71°52'43"E/35°38'24"N							
1	649	30.814 ± 0.002	0.080 ± 0.001	0.012 ± 0.001	0.135 ± 0.004	0.075 ± 0.001	151.7 ± 4.4
2	890	98.728 ± 0.005	0.351 ± 0.001	0.057 ± 0.001	1.525 ± 0.006	0.146 ± 0.001	217.7 ± 1.2
3	930	39.827 ± 0.004	0.170 ± 0.001	0.028 ± 0.001	1.560 ± 0.011	0.032 ± 0.001	246.0 ± 2.5
4	970	52.294 ± 0.003	0.400 ± 0.001	0.079 ± 0.001	2.186 ± 0.008	0.024 ± 0.001	158.8 ± 0.7
5	988	88.635 ± 0.013	0.835 ± 0.001	0.157 ± 0.001	3.924 ± 0.012	0.022 ± 0.001	138.9 ± 0.4
6	1005	90.851 ± 0.024	0.913 ± 0.001	0.168 ± 0.001	4.229 ± 0.012	0.021 ± 0.001	131.2 ± 0.4
7	1025	88.582 ± 0.010	0.925 ± 0.001	0.160 ± 0.001	4.221 ± 0.014	0.018 ± 0.001	127.6 ± 0.5
8	1045	90.116 ± 0.013	0.959 ± 0.001	0.156 ± 0.001	4.341 ± 0.013	0.018 ± 0.001	125.2 ± 0.5
9	1068	70.295 ± 0.015	0.751 ± 0.001	0.116 ± 0.001	3.432 ± 0.010	0.017 ± 0.001	123.5 ± 0.5
10	1107	61.509 ± 0.010	0.613 ± 0.002	0.104 ± 0.001	3.007 ± 0.012	0.011 ± 0.001	134.2 ± 0.5
11	1158	78.290 ± 0.005	0.745 ± 0.001	0.136 ± 0.001	3.689 ± 0.012	0.018 ± 0.001	138.1 ± 0.4
12	1208	18.544 ± 0.000	0.168 ± 0.001	0.027 ± 0.001	0.833 ± 0.006	0.002 ± 0.001	150.4 ± 2.6
13	1441	107.241 ± 0.013	1.005 ± 0.001	0.178 ± 0.001	4.983 ± 0.015	0.031 ± 0.001	138.1 ± 0.4
01B24 (48.3 mg; J = 0.805*10-3; Ar* = 2089; K20 = 1.23; CaO = 17.5; Cl = 618)							
1	645	53.919 ± 0.042	0.229 ± 0.007	0.023 ± 0.008	1.170 ± 0.05	0.111 ± 0.007	129.9 ± 12
2	908	84.312 ± 0.011	0.799 ± 0.008	0.192 ± 0.004	5.020 ± 0.06	0.112 ± 0.005	91.4 ± 2.8
3	969	170.201 ± 0.018	3.099 ± 0.011	1.109 ± 0.008	20.43 ± 0.10	0.133 ± 0.006	61.0 ± 0.8
4	990	324.508 ± 0.063	7.516 ± 0.010	2.734 ± 0.010	47.65 ± 0.15	0.130 ± 0.007	55.0 ± 0.3
5	997	163.088 ± 0.038	4.125 ± 0.010	1.450 ± 0.008	24.92 ± 0.09	0.052 ± 0.007	51.8 ± 0.6
6	1002	72.460 ± 0.003	1.789 ± 0.005	0.633 ± 0.005	10.47 ± 0.05	0.046 ± 0.006	47.6 ± 1.4
7	1013	42.202 ± 0.007	0.961 ± 0.007	0.311 ± 0.009	5.49 ± 0.05	0.036 ± 0.007	47.7 ± 2.8
8	1023	30.882 ± 0.001	0.604 ± 0.009	0.178 ± 0.005	3.55 ± 0.06	0.049 ± 0.007	39.5 ± 4.6
9	1032	30.267 ± 0.015	0.521 ± 0.007	0.178 ± 0.010	3.54 ± 0.05	0.025 ± 0.007	63.6 ± 5.7
10	1045	49.272 ± 0.019	0.991 ± 0.006	0.343 ± 0.005	6.42 ± 0.05	0.005 ± 0.007	69.1 ± 2.1
11	1075	154.391 ± 0.098	3.786 ± 0.010	1.371 ± 0.006	23.99 ± 0.10	0.080 ± 0.006	50.0 ± 0.6
12	1105	222.864 ± 0.056	5.487 ± 0.009	1.994 ± 0.009	34.98 ± 0.12	0.088 ± 0.006	51.9 ± 0.4
13	1159	376.300 ± 0.147	9.774 ± 0.012	3.568 ± 0.012	60.22 ± 0.18	0.106 ± 0.006	51.1 ± 0.2
14	1208	288.420 ± 0.070	7.620 ± 0.011	2.732 ± 0.010	46.83 ± 0.16	0.089 ± 0.006	49.8 ± 0.3
15	1316	263.370 ± 0.000	6.971 ± 0.013	2.440 ± 0.007	42.23 ± 0.14	0.104 ± 0.006	48.4 ± 0.3
16	1435	131.600 ± 0.002	3.276 ± 0.012	1.140 ± 0.008	20.05 ± 0.10	0.081 ± 0.006	47.7 ± 0.8

best estimate for the dyke emplacement. The discordance can be explained by mixing inherited Paleozoic and Proterozoic zircon cores with Eocene rims. The εHf values of the discordant zircons scatter between –5.6 and +2.5 (Table 2). They do not show a systematic trend with the age of the inherited component. However, analysis 30, closest to the lower intercept age of 47.4 ± 0.5 Ma, yielded the most negative εHf value (-5.6) and is regarded as best reflecting the hafnium composition of the granite intrusion.

Granite dyke (01A07)

This undeformed dyke intruded meta-gabbros and –diorites of the Kohistan Arc (Fig. 19). The sample was taken 1 km south

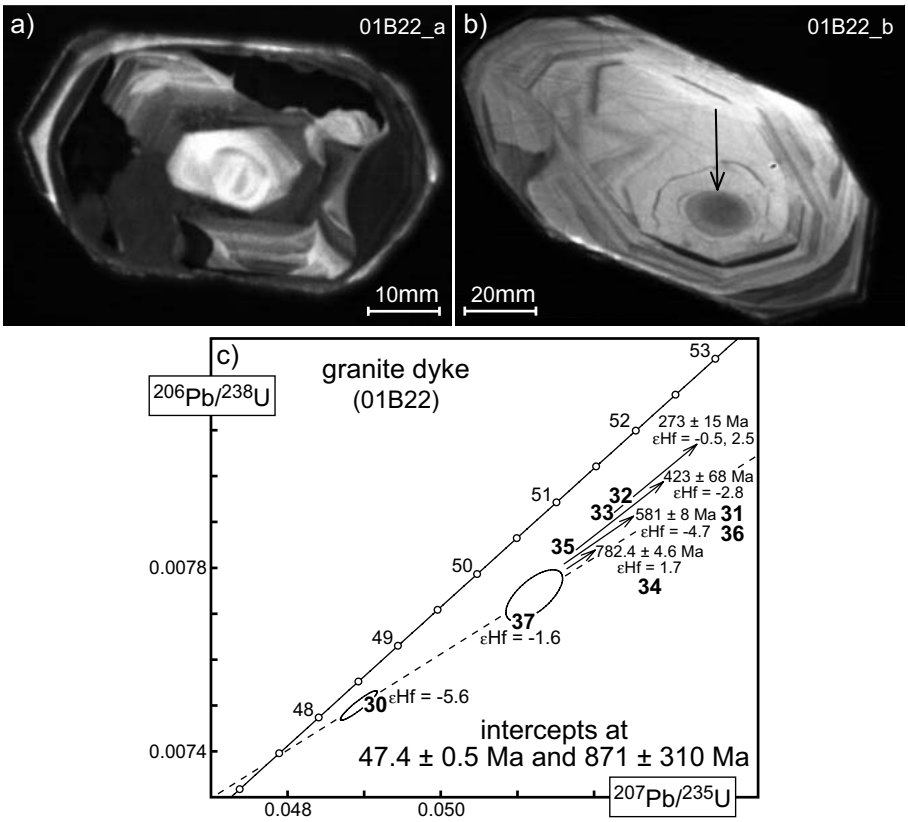

Fig. 18. Zircons of the granite dyke (01B22); a) and b) Cathodoluminescence images; arrow in b points to a small inherited core; c) U-Pb Concordia diagram. GPS point and analytical data in table 3.

of the granite sample 01B22. It comprises magmatic quartz, microcline, plagioclase ± biotite ± titanite and muscovite as alteration product. Cathodoluminescence images of zircons display undisturbed, oscillatory zoning patterns (Fig. 20a) as well as polyphase textures in the core with an undisturbed zoning pattern at the margins (Fig. 20b).

Five zircon microfractions with 2 to 4 grains were analysed (Table 3, Fig. 20c). Four microfractions yielded $^{206}Pb/^{238}U$ ages between 38.5 and 40.0 Ma whereas microfraction 42 was dated at 49.0 Ma ($^{206}Pb/^{238}U$ age). An upper intercept age of 293 ± 93 Ma and a lower intercept at 37.4 ± 2.5 Ma were calculated from all five points. A mean $^{206}Pb/^{238}U$ age of 38.73 ± 0.20 Ma was obtained from three youngest microfractions (30, 40 and 41) and is interpreted as maximum intrusion age since the points may still be biased by inheritance, despite their apparent concordancy.

The zircon fractions 38, 39, 40, 41 yielded εHf values between +8.3 and +11.2 with a mean of +9.4 ± 3.8 derived from the three concordant fractions (38, 40, 41; Table 2), whereas analysis 42 has a significantly lower εHf value (+5.8) reflecting the inherited component with a crustal hafnium signature.

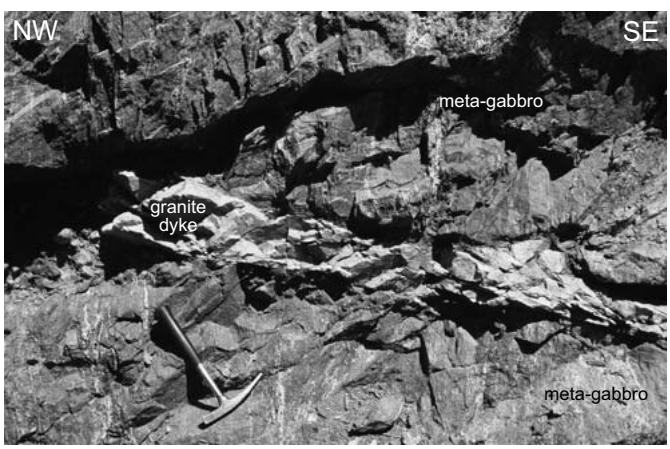

Fig. 19. Granite dyke (01A07) intrusive into and crosscutting the foliated the meta-gabbros and -diorites of the Kohistan Arc at the sampling site (GPS in table 3).

^{39}Ar-^{40}Ar age determinations

Tirich Mir granite (ZP22)

^{39}Ar-^{40}Ar data were obtained on a small aliquot of ZP 22 muscovite. The results are shown in table 5 and figure 21. The K concentration of 5.8% is not stoichiometric, as the ^{39}Ar production indicates pervasive alteration. Therefore, interpreting the step-heating data must take into account this secondary "chemical event".

The explanation of the hump-shaped age spectrum (Fig. 21a) may require a mixture between two diachronic mineral generations (Wijbrans and McDougall, 1986). To unravel heterochemical mixtures, it is useful to take into account the Cl/K

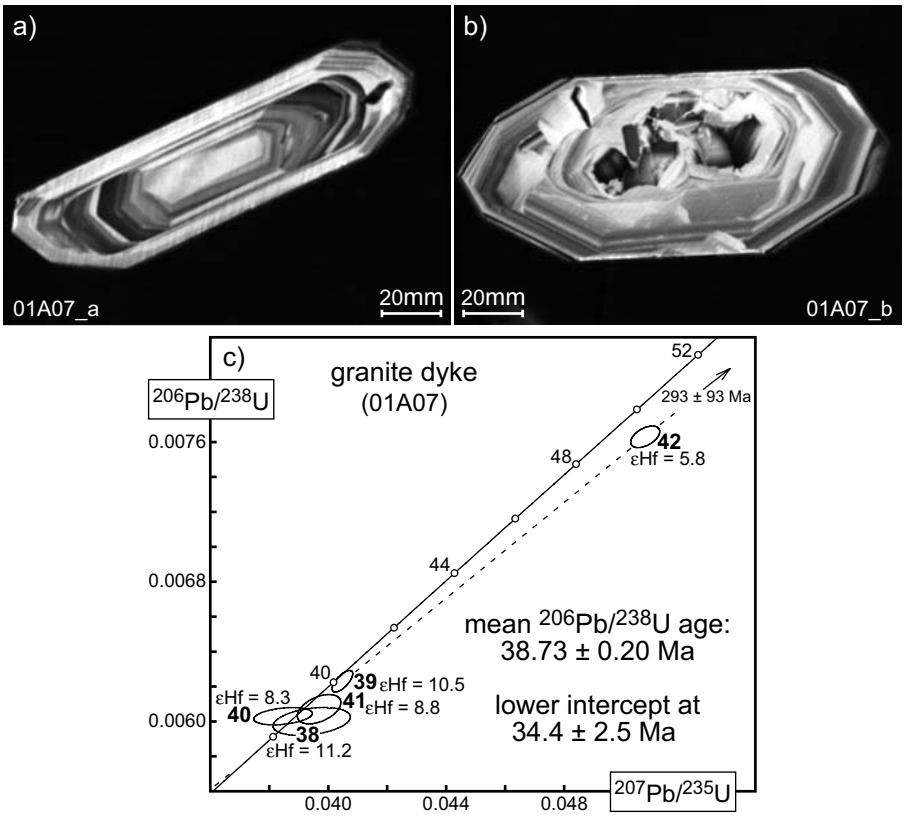

Fig. 20. Zircons of the granite dyke (01A07); a) and b) Cathodoluminescence images; c) U-Pb Concordia diagram. GPS point and analytical data in table 3.

Tab. 5. Ar-Ar stepwise heating results, keys as in Table 4.

Step	T (°C)	$^{40}Ar_{tot}$	^{39}Ar	^{38}Ar	^{37}Ar	^{36}Ar	Age ± 1σ Ma
ZP 22 (8.7 mg, J = 0.001085, Ar* = 24308, K2O = 6.96, CaO = 0.38, Cl = 33)							
1	520	449.7±0.1	3.43±0.02	0.32±0.02	0.45±0.05	1.12±0.03	65.2±3.7
2	614	1577.6±0.9	22.52±0.03	0.80±0.02	0.87±0.04	1.84±0.03	89.2±0.6
3	700	1797.3±0.6	26.90±0.06	0.48±0.02	0.30±0.05	0.87±0.01	108.7±0.3
4	750	4480.3±1.4	71.42±0.07	1.09±0.01	0.44±0.03	1.21±0.03	109.6±0.2
5	830	2625.9±0.3	40.02±0.05	0.74±0.01	0.56±0.04	1.01±0.02	110.8±0.3
6	920	1687.1±0.8	25.97±0.03	0.53±0.01	0.84±0.03	0.82±0.01	105.8±0.3
7	1120	2939.7±1.7	45.83±0.07	0.85±0.02	1.34±0.04	1.20±0.03	107.2±0.4
8	1370	1482.9±0.4	23.41±0.02	0.56±0.01	1.26±0.04	0.99±0.02	96.3±0.4

ratio (Villa et al., 1997). The data points of muscovite ZP 22 define a linear anticorrelation between apparent step age and Cl/K ratio (Fig. 21b). We attribute the steps with highest Cl/K ratios to the obvious alteration phases; lowest Cl/K ratios corresponding to the highest ages are interpreted as the least altered phase. A regression through the linear array intercepts the ordinate axis (i.e. Cl/K = 0) at an age of 110.6 ± 3.2 Ma. This modelled muscovite age is broadly consistent with the U-Pb intrusion age obtained in the present work. The ca. 10 Ma difference between the zircon and white mica apparent ages deserves some discussion. The conventional "cooling age" explanation is difficult to accept because the shallow intrusion depth of the Tirich Mir pluton excludes "cooling" longer than 0.1 Ma. Two explanations are conceivable: muscovite records post-magmatic recrystallisation, while the zircon age is accurate; or, the three zircon analyses are shifted parallel to the concordia by a small, undiagnosed inherited core and the muscovite records the true magmatic episode. Owing to the sub-stoichiometric chemical composition of the muscovite, the first explanation is more likely.

These ^{39}Ar-^{40}Ar results are sufficiently clear to infer that the ca. 140 Ma apparent Rb-Sr age (Villa et al., 2001) is incorrect, due to alkali mobility during a chemical open-system event. This is supported both by the fact that the two Rb-Sr whole-rock analyses defined a two-point isochron age of 14.9 ± 1.8 Ma, and by the sub-stoichiometric chemical composition of muscovite.

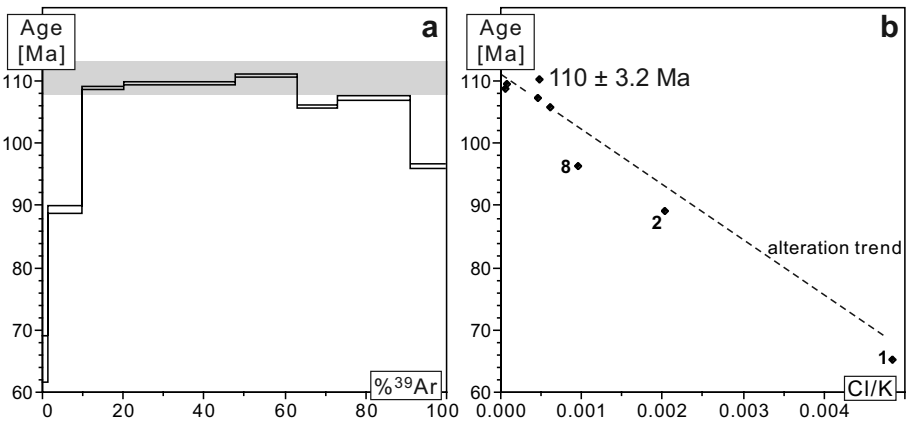

Fig. 21. ^{39}Ar-^{40}Ar results from Tirich Mir muscovite ZP22. a) Hump-shaped age spectrum. (b) Cl/K vs. age diagram whose negative correlation confirms the mixing of Cl-poor muscovite with a young, Cl-rich alteration phase. Grey bar in (a): Age estimate representing the intercept of the alteration trend with the ordinate axis in (b).

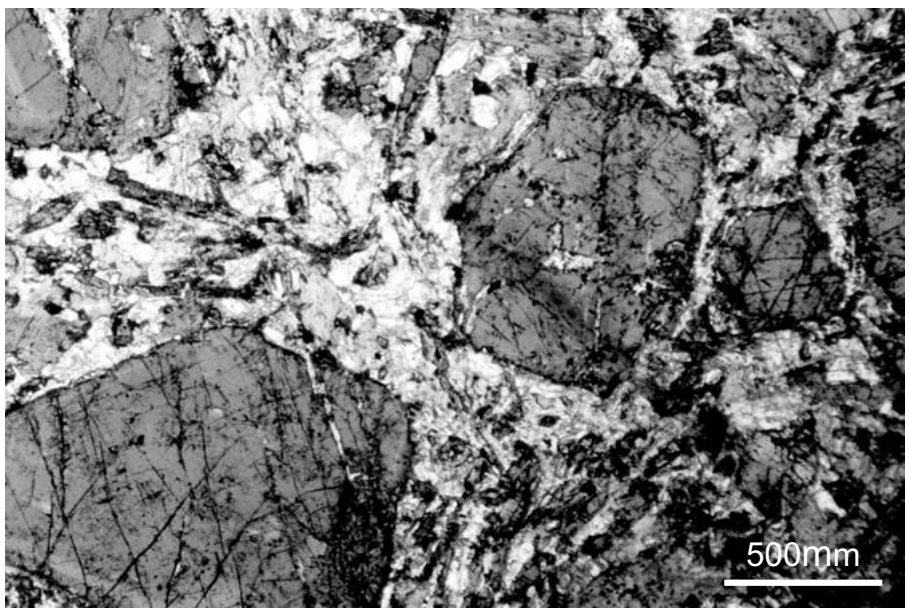

Fig. 22. Thin section of the 20.1 basalt sill showing euhedral amphibole phenocrysts used for Ar-Ar dating in this work. GPS point in table 2.

Basalt sill (20.1)

Ar-Ar analyses were carried out to support the U-Pb results and to exclude the possibility of cross-contamination by zircons of another sample during preparation of the 106.64 ± 0.35 Ma basaltic sill, which yielded only 12 zircons (sample weight 0.85 kg). Brown magmatic and green euhedral amphiboles occur as phenocrysts (Fig. 22). Green amphibole grew along rims of brown amphibole and is altered to calcite, muscovite and epidote. The rock matrix consists of brown, smaller grained amphibole and mainly alteration products. The hand-picked amphiboles mainly represent the brown, likely magmatic phase. However, alteration products occur in all of the separated amphibole grains and could not entirely be removed during hand picking.

Four temperature steps (steps 10 to 13) between 1060 and 1160 °C released gas with a uniform chemical signature and Ca/K ratios between 11.6 and 12.0 and Cl/K ratios between 0.021 and 0.025 (Fig. 23a). These four "isochemical" steps account for 62% of the total Ar release (Fig. 23b). A weighted mean age of 106.8 ± 2.5 (2σ error) was calculated from the four isochemical steps 10 to 13, (T = 1077 to 1160 °C), confirming the 106.64 ± 0.35 Ma U-Pb zircon age (Fig. 23c). Two further steps (8 and 9, 1040 and 1057 °C) have chemical signatures close to the four steps 10-13; calculating the weighted average on all six steps gives 107 ± 2 Ma, indistinguishable from the previous one and from the U-Pb age. The other steps probably represent extraneous (alteration?) phases, as demonstrated by their heterochemical Ca/K and Cl/K ratios and discordant step ages.

Quartz-monzodiorite (01B16)

Meta-harzburgitic serpentinite is enclaved in a quartz-monzodiorite in the Tar Gol (Fig. 24). No zircon could be separated from the 24 kg sample whose magmatic minerals are magnesio-hastingsite, ilmenite, plagioclase, quartz, possibly garnet

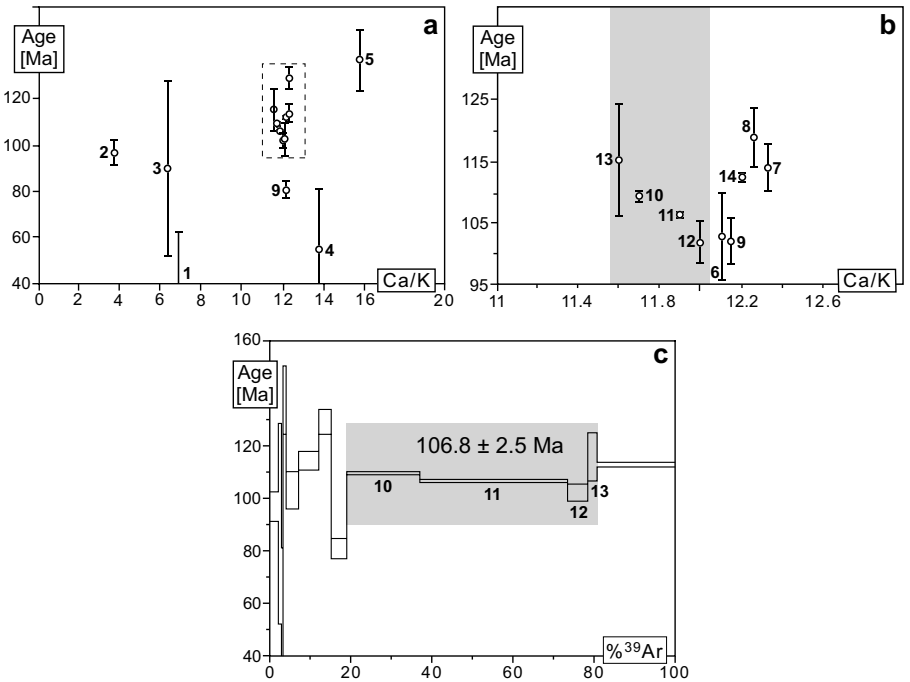

Fig. 23. ^{39}Ar-^{40}Ar results from amphiboles of basalt sill 20.1; a) Three-isotope correlation diagram. The dashed around Ca/K= 12 is taken to represent the true amphibole and is expanded in figure b; 1 to 14 = step numbers. b) Detail of (a): the grey box identifies the steps with Ca/K = 11.8 ± 0.2, used to estimate the age of amphibole. c) Age spectrum; the grey box, containing 61% of the total Ar, is defined by the four steps highlighted in (b).

and accessory apatite. The rock is strongly altered to fine-grained unspecified feldspar, epidote, titanite and chlorite. Magmatic magnesio-hastingsite has cores of a dark green amphibole that could not be removed during separation and hand picking. The separated amphibole fraction contains a significant amount of alteration products (e.g. chlorite, feldspar, titanite) and cores of green amphibole.

Steps number 5 to 9 appear to define a linear trend in both Cl/K-Ca/K and age-Ca/K correlation plots (Fig. 25a and b). This suggests that these steps represent a binary mixing of two gas-rich phases, e.g. two amphibole generations. The temperature steps 10 to 13 seem to represent the addition of a more Ca-rich, excess Ar bearing, contaminant (pyroxene?). Three electron microprobe analyses (EMP) yielded Ca/K ratios of 8.19, 9.15 and 9.25, highlighted by the black bars in the horizontal dark grey box near the abscissa in Fig. 25a. Two EMP measurements were done at the rims of such an amphibole grain.

As mentioned above, steps 5 to 9 likely represent mixing, on account of their correlated variations in Ca/K, Cl/K and age. The two end-members have for one, Ca/K ≥ 9.43 ± 0.03 and an apparent age ≥ 138.9 ± 0.4 Ma; for the other, Ca/K ≤ 9.08 ± 0.03 and an apparent age ≤ 125.2 ± 0.5 Ma. The leftmost point on the trend line, step 8, could be viewed as the closest representative of the magmatic amphibole reservoir, which thus would be assigned an age of 125.2 ± 0.9 Ma.

The measurement yielding 8.19 was measured in the core of a euhedral magnesio-hastingsite and is therefore interpreted as the value for the primary magmatic phase. In this case, the lowest obtained Ca/K ratio (= 8.19) would be representative for the primarily magmatic hornblende, an Ar-Ar age of about 90 Ma may be estimated from the extrapolation of the binary mixing line to such a value (Fig. 25a). However, the long extrapolation is based on one single EMP data point, out of a total of three, whose statistical representativity is uncertain. Thus, only first-order chronological information ("between 90 and 130 Ma") can be constrained at the present stage due to our limited knowledge of microchemistry, despite the good precision of the Ar-Ar analyses.

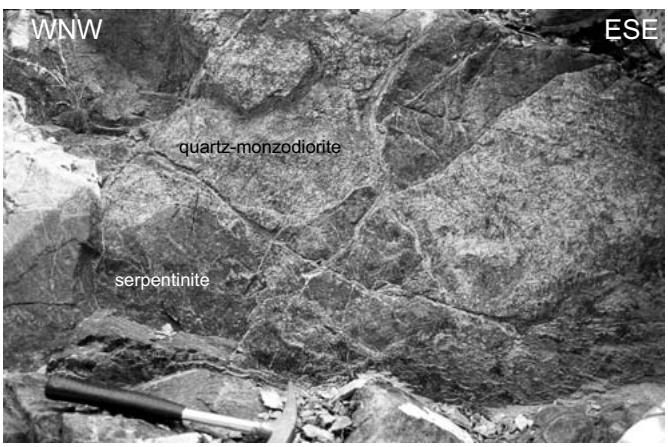

Fig. 24. Enclaves of serpentinised harzburgites in the 01B16 quartz-monzodiorite. GPS point in table 4.

Meta-gabbro (01B24)

The 49.80 ± 0.15 Ma U-Pb age of the 01B24 meta-gabbro was obtained from only one concordant zircon microfraction

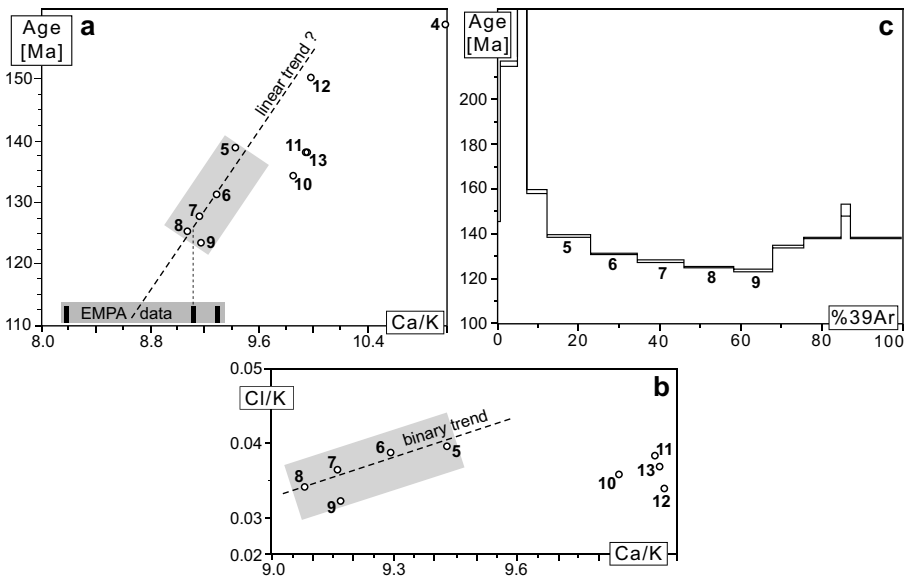

Fig. 25. ^{39}Ar-^{40}Ar results from the quartz-monzodiorite 01B16; a) Three-isotope correlation diagram. The dark grey box represents the amphibole EMP analyses. The light grey box along the trend line identifies the steps interpreted as the mixture of two amphibole generations. Labels represent the step numbers. The vertical dotted segment identifies step 8 as closest to the EMP analysis. (b) Ca-Cl-K three-element correlation diagram. The grey box highlights a binary mixing trend (Villa, 2001) defined by the same five steps as in (a). (c) Age spectrum. The grey box highlights the steps proposed to represent the two amphibole generations identified in (a) and (b). The average age of the mixture, 130 ± 7.6 Ma, has no geological significance.

(Fig. 16). To support this intrusion age, Ar-Ar dating was carried out on tschermakitic hornblende. Metamorphic minerals (biotite, actinolite, epidote and chlorite) that are locally over- and intergrown with the magmatic hornblende could not completely be removed from the hand-picked, analysed fraction.

A small but prominent irregularity in the ^{39}Ar-age spectra (Fig. 26b) is produced by the steps 8, 9 and 10. They degassed between 1023 and 1045°C and account together for only 3.7% of total Ar released and are thus interpreted as actinolite or chlorite phases (high Ca/K; steps 9, 10) or other alteration products (step 5, Fig. 16a). All steps to the left of that peak (degassing below 1023°C) do not seem to represent the primarily magmatic tschermakitic hornblende. Steps 11 to 16 have relatively uniform Ca/K ratios between 12.17 and 12.80, and correspondingly their step ages, accounting for 64% of the total, do not show much variation (almost satisfying a plateau definition). Therefore, these steps are interpreted to date the magmatic, tschermakitic hornblende and a weighted mean age of 50.2 ± 1.4 Ma was calculated from these six steps, consistent with the 49.80 ± 0.15 Ma U-Pb age. A subset of these six steps, chosen to reduce the dispersion of the Ca/K ratio (12.17 to 12.50), includes steps 13 to 16 and yields a weighted average of 50.0 ± 2.1 Ma. This age is indistinguishable from both the six-step average and the U-Pb age and underscores the robustness of the Ar-Ar age. Furthermore, this age reveals that the two intermediate zircon fractions 27 and 29 (Fig. 16) reflect mixing of the 49.8 Ma age and a younger event at 44.2 Ma.

Melt sources in Karakoram and Kohistan units

The high field strength elements (HFSE) Nb, Ta, Zr, Hf and Ti, were considered to be type examples of so-called 'conservative' elements, which are essentially immobile during slab dehydration (Pearce and Peate, 1995). Thus, HFSE should not be influenced by the subducting slab and would provide an insight into the pre-subduction nature of the mantle-wedge. However, sedimentary hafnium has contributed to arc lavas (Antilles and Sunda arcs) and can be transferred from the subducting slab to the mantle wedge (Woodhead et al., 2001). This potential mobility of Hf derived from slab sediments should therefore be taken into account when interpreting the initial Hf isotopic ratios of zircon analysed in this study. They show a restricted range of positive values between +2 and +15 for zircons devoid of inheritance (Table 2), pointing to a dominant depleted mantle origin of the Hf (with values up to εHf = +15), but however with some sedimentary slab component involved, a case being characteristic for modern and ancient arcs (Schaltegger et al., 2002). The values are attributed to processes acting during the Neo-Tethys subduction along the active Karakoram margin and the Kohistan oceanic island arc. The hafnium isotopic compositions represent intermediate values between continental crust signature (-10 < εHf < -20, Vervoort et al., 1999; Vervoort et al., 1996) and a depleted mantle signature (+15 < εHf < +25, Patchett and Tatsumoto, 1980; Nowell et al., 1998; Chauvel and Blichert-Toft, 2001).

Karakoram and suture zone

The εHf values of the six 112 to 104 Ma intrusions from the three distinct tectonic units show an apparent increase from the Karakoram through the Suture to the Kohistan (Fig. 27).

The 107 Ma old quartz diorite (sh2500) and granite dyke (01A50b) occur within the suture zone, but they intruded Karakoram shelf-type volcanogenic sediments that are now imbricated in the suture. Reassigning these two intrusions to the Karakoram terrane makes the hafnium isotopic contrast between Karakoram and suture smaller, but does not affect the contrast between Karakoram and suture intrusions on the

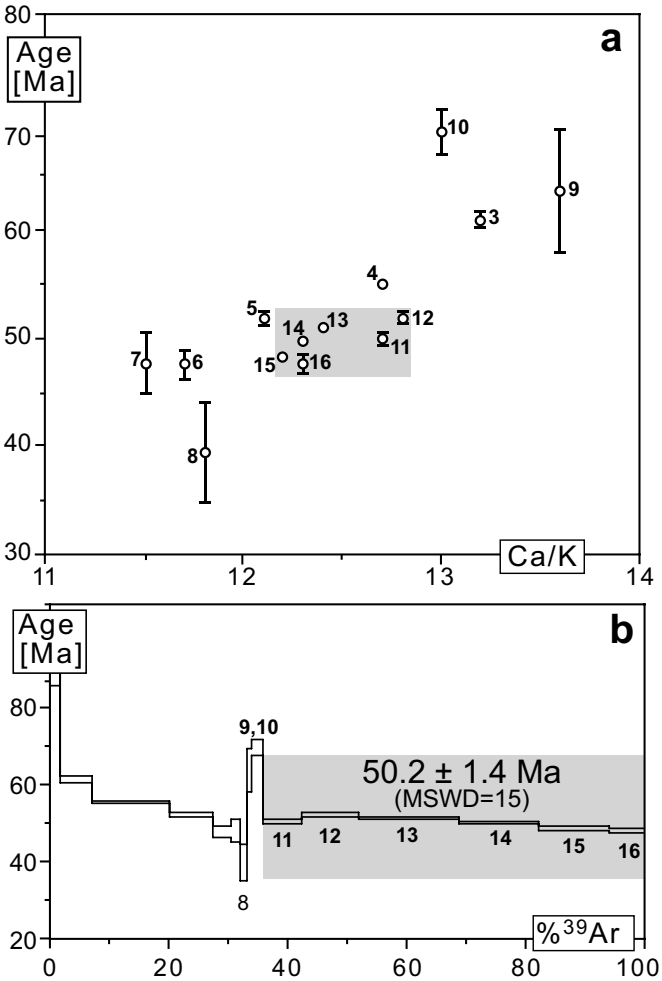

Fig. 26. ^{39}Ar-^{40}Ar results from hornblende of meta-gabbro 01B24; a) Three-isotope correlation diagram. The grey box highlights steps having Ca/K ratios around 12.5, corresponding to magmatic hornblende. (b) Age spectrum. The steps identified as hornblende in (a) contain 63% of the total Ar and define an isochemical age of 50.2 ± 1.4 Ma.

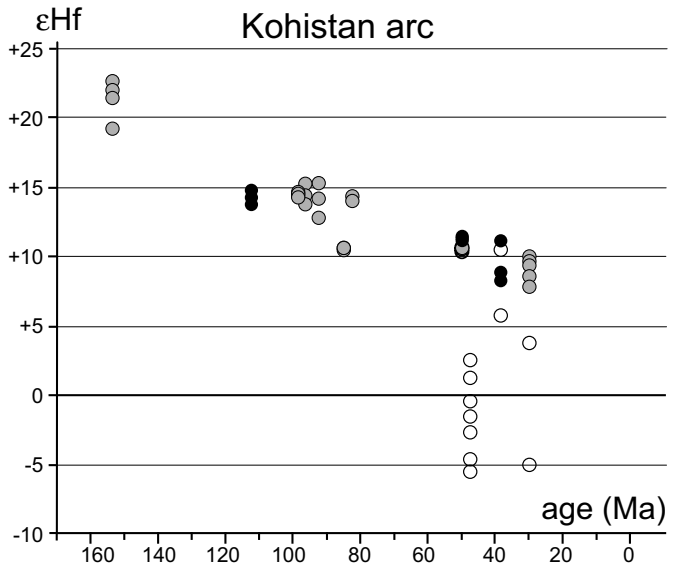

Fig. 27. Initial εHf vs. age plot of samples from the Kohistan paleo-island arc, showing an evolution from εHf values of +24 to c. +10 with time (only for the concordant magmatic zircons). Black dots: magmatic zircons from this study; white dots: inherited zircons (this study); grey dots: samples from (Schaltegger et al., 2002), and work in progress (mentioned in Schaltegger et al., 2003).

one hand (εHf = +2 to +11), and the northern Kohistan diorite on the other hand (εHf +14). The variable εHf values of the four near-coeval (107 to 104 Ma old), calc-alkaline Karakoram samples imply a hybrid melt composition derived from different mantle and crust-derived sources.

The only 'true' suture zone sample, the 107 Ma basalt sill, has an εHf value (+10) fitting the range of values obtained for the Karakoram samples (Fig. 27).

Kohistan intrusions

The εHf values of the Kohistan samples decreases from +14.6 to +8.3 with time when one considers the concordant microfractions only (Fig. 27). This decrease is even stronger, when one includes εHf = +24 of 154 Ma diorites from north-eastern Kohistan (Schaltegger et al., 2003) and work in progress). Melts that formed the Kohistan Arc seem to have tapped an increasingly enriched mantle source.

The oldest rocks of the Kohistan reflect εHf values that are typical for MORB-type mantle, e.g., the Mirkhani diorite with an εHf of +14.3. For comparison, present-day Indian MOR basalts have εHf between +11 and +22 (Nowell et al., 1998; Chauvel and Blichert-Toft, 2001). Calc-alkaline, early to recent arc volcanic rocks of the Izu-Bonin-Mariana system yield +14.2 < εHf < +19.0 and tholeiitic to calc-alkaline basalts of the so-called Proto-arc, formed during initiation of subduction, have slightly lower values, between +12.2 and +17.6 (Pearce et al., 1999). Alternatively, contributions of recycled lower crust of the island arc (Nowell et al., 1998) and/or a slab component (oceanic crust or sediments in the mantle wedge (Woodhead et al., 2001) may explain εHf (+13 to +15) slightly lower than typical MORB-type values (εHf > +15). Oceanic sediments may have strongly varying hafnium isotopic ratios from +14 (deep-sea turbidites) or +6 (pelagic sediments) to extremely enriched ratios around -20 to -40 (Vervoort et al., 1999; Godfrey et al., 1997; Albarède et al., 1998). It is therefore difficult to make a more quantitative assessment on slab contributions on the basis of Hf isotopes only.

The three Eocene Kohistan intrusions (dated at 50-39 Ma) are younger than collision of Kohistan with India (65-50 Ma). The εHf values of both the 50 Ma old meta-gabbro (+11.6) and the 39 Ma old granite dyke (+9.4) point to a less depleted melt source than MORB-type mantle. Eocene to Proterozoic inherited zircons within the 47 Ma old granite dyke with variable εHf values between -5.6 and +2.5 reflect the composite zircons

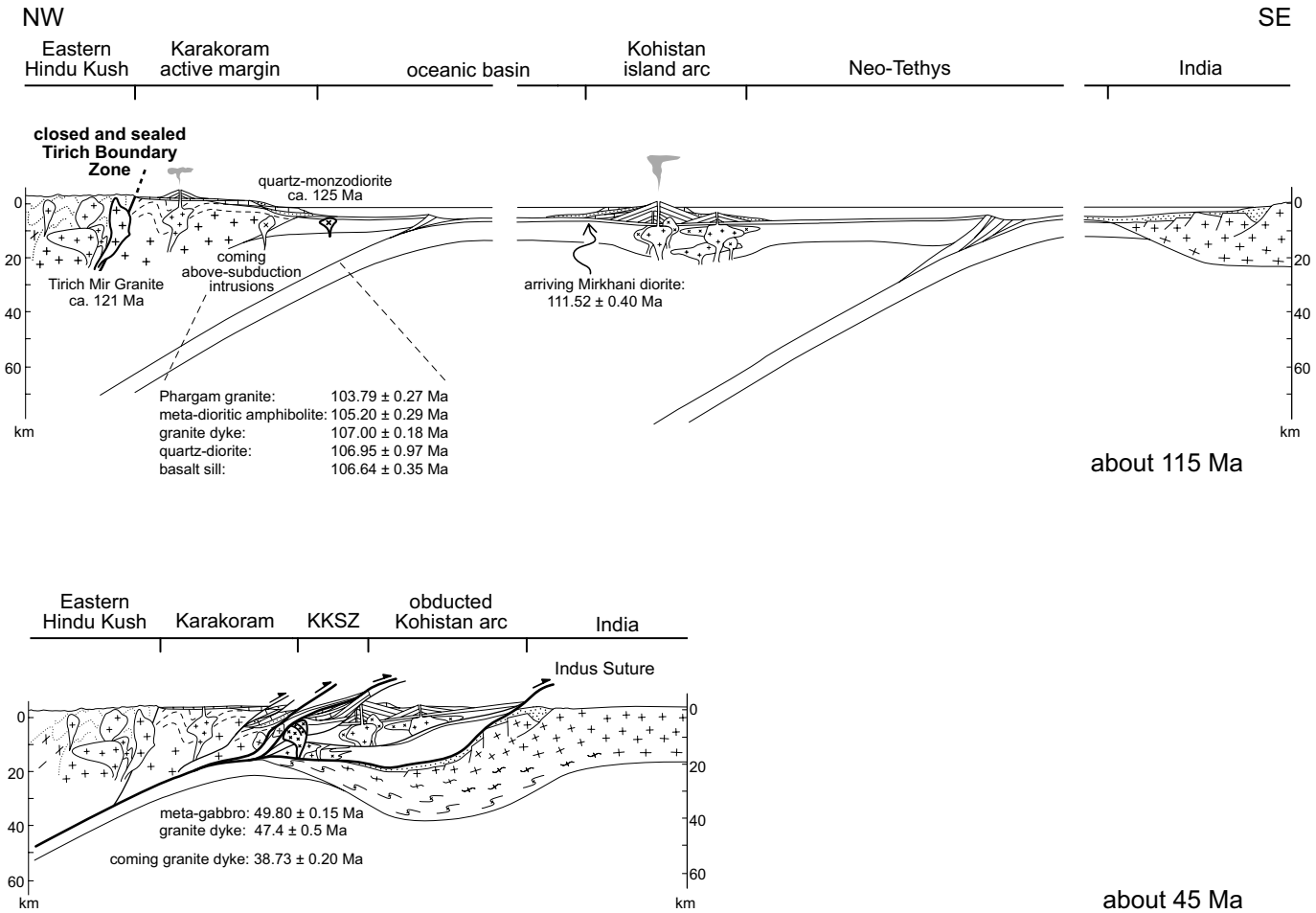

Fig. 28. Plate tectonic interpretation summarising the geological context of the new geochronological information (this work). Post 45 Ma imbrication will involve dominant strike-slip faulting in the KKSZ. Sketches omit penetrative deformation structures in order to identify the major tectonic units (Karakoram-Kohistan-India).

population derived from several phases of melting and crystallisation in a continental crust since the Proterozoic. These zircons are attributed to either a Proterozoic continental crust or clastic sediments now subducted below the Kohistan Arc. Three leucogranitic dykes (01B22, 01A77 and a leucogranite at the Indus confluence; Schaltegger et al., 2003) have ages between 47 and 30 Ma and values between +8 and +11 for concordant zircons, but a significant crustal inheritance with εHf down to -6 in inherited discordant zircons (Fig. 27). Grossly coeval dykes are therefore tapping different melt sources at about the same time, or possibly sampling and assimilating different types of crust.

Plate tectonics interpretation

The U-Pb zircon ages of ten tholeiitic to mainly calc-alkaline intrusions on both sides of the suture are used to constrain the history of the Karakoram-Kohistan Suture Zone.

The five diorites and granites of the Karakoram Terrane are partly imbricated in the suture zone and represent subduction-related magmatism at the active continental Karakoram margin. Inherited zircons of Proterozoic age (ca. 725 to 1620 Ma) are likely derived from the Karakoram crust that formed a part of the Gondwana supercontinent before the Late Paleozoic. As a regional comparison, Indian plate gneisses in the footwall of the Indus Suture yielded U-Pb ages of 1864 Ma (DiPietro and Isachsen, 2001) and 1858 Ma (Zeilinger, 2002). Hafnium isotopic ratios show a varying melt composition somewhere between a crustal end member and a depleted (MORB-type) mantle source and thus fit a continental margin setting. They further confirm lithological and petrological interpretations that two intrusions (01A50b and sh2500) in the suture zone are Karakoram-related as they have εHf values in the same range of +2 to +11.

The only 'true' suture zone sample, the 107 Ma basalt sill (20.1), has a hafnium isotopic composition (εHf of +10) similar to the imbricated Karakoram samples, and thus seems to represent the same subduction-related magmatism at the Karakoram margin.

Almost contemporaneous island arc magmatism in north-

western Kohistan is documented by Aptian (125-112 Ma) andesites that were intruded by the 112 Ma Mirkhani diorite. A melt source close to MORB-type composition is inferred for that diorite, as well as for younger Kohistan intrusions (100-80 Ma; Schaltegger et al., 2002), distinctly different from the Karakoram melts. The 50 Ma Kohistan, tholeiitic meta-gabbro is thought to represent partial melting of a depleted mantle (near-MORB-type) in the mantle wedge below the Kohistan Arc. At that time, the mantle wedge may have been very thin above the already underthrust Indian crustal slab (Kaneko et al., 2003). The slightly younger, 47 Ma granite dyke intruding this meta-gabbro is derived from a completely different, crustal source. The inferred youngest upper intercept age of 273 ± 15 Ma for the inherited zircons fits the 269 Ma U-Pb zircon age of Indian Plate Kaghan eclogites in NE Pakistan (Tonarini et al., 1993). The Paleozoic and Proterozoic zircons are likely derived from Gondwana crust or detrital, subducted sediments underlying the KKSZ and northernmost Kohistan in the early Eocene.

Conclusion

The geochronological evidence presented in this paper is consistent with Cretaceous subduction beneath the Karakoram Terrane. The Tirich Mir granite is a product of the subduction-related Cretaceous magmatism responsible for the Karakoram Batholith, although this pluton is geographically separated from the main intrusions. The new age determinations also confirm that accretion of the Karakoram Terrane to the Eurasian margin along the Tirich Boundary Zone is older than 120 Ma. Geochronological data further suggest that the rocks now imbricated in the Karakoram-Kohistan Suture are mostly derived from the Karakoram (overriding) plate. In particular, ultramafic rocks of the Karakoram passive margin were serpentinised before Cretaceous calc-alkaline magmatism. These serpentinites likely floored the Karakoram forearc region during Cretaceous times, and possibly earlier. If there was any oceanic lithosphere in the North-Kohistan oceanic basin, the related ophiolites have been subducted beneath the Karakoram active margin. The related calc-alkaline magmatism seems to have stopped at about 100 Ma, which would be the age of the cessation of subduction below the Karakoram Terrane (early collision with Kohistan?). However, this age does not signal the end of tectonic activity along the suture and within the Kohistan Arc.

Deformed granite dykes on the Kohistan side show that the magmatic and tectonic history of the Karakoram-Kohistan Suture Zone was not finished by 75 Ma, as most models assume, but continued to Eocene times. Tectonic and magmatic processes in the arc plates were more complex and long-lasting, possibly due to complex and few million year long interplays between subduction and thrusting events in the forearc, within-arc and back-arc regions between two active subduction zones (Boutelier et al., 2003). Inherited cores in the Eocene intrusions suggest that the Indian northern margin was underthrust as far as the northern part of the presently exposed Kohistan Arc.

Initial hafnium isotopic compositions in zircon reflect the evolution of the magma source area. In particular, some magmas participating to the construction of the arc were derived from the re-melting of its deep crust, likely as a response to crustal thickening during magmatic accretion.

Acknowlegements

These results are part of the PhD thesis of the senior author supported by the ETH, grant N° 20-884-01. J.P.B., U.S. and M.F. thank the Swiss National Science Foundation for supporting their scientific work. The National Museum of Natural History in Islamabad supported field work for S.H. and H.D. Technical support by U. Gerber, I. Ivanov and A. von Quadt are kindly acknowledged. J. Di Pietro and M. Whitehouse provided valuable reviews that help clarifying several points of this work.

Appendix

U-Pb age determinations

Analytical procedures include isotope dilution thermal ionisation mass spectrometry (ID-TIMS).
Samples of 1 to 24 kg of fresh rock were crushed and zircons were separated from a fraction smaller than 350 µm using conventional mineral concentration procedures and equipment including a jaw-crusher, disk mill, Wilfley table and heavy liquids (methylene iodide). The non-magnetic zircon fraction, separated by a Frantz magnetic separator, was hand-picked under a binocular microscope (Krogh, 1982b). According to morphological criteria, colour and the presence of cracks, cores and impurities, single grains or microfractions were selected. The zircons were air-abraded (if not, mentioned in tables 1 and 3) to eliminate zones of marginal lead loss (Krogh, 1982a). The removal of the zircon margins reduced the common Pb contents and improved concordance. The selected zircons were then washed in 4 N nitric acid and rinsed several times with distilled high-purity water and distilled acetone in an ultrasonic bath. Dissolution in HF-HNO_3, chemical separation on anion exchange resin and mass spectrometry followed standard techniques (Krogh, 1973) but with ion-exchange columns downsized at 1/10 of the original columns. U and Pb were loaded on a single Rhenium filament with H_3PO_4 and silica gel. Isotopic ratios were measured on a Finnigan MAT 262 system (at ETH Zürich) equipped with an ion counting system. The accuracy of the ion counting system was monitored by repeated measurements of the NBS 982 standard and corrected for fractionation with 0.09%/amu. The procedural lead blank was estimated at 0.6±0.3 pg. Common lead concentration in excess of the blank lead were mostly corrected using crustal lead isotopic compositions (Stacey and Kramers, 1975), but using depleted mantle compositions for zircon populations with εHf values of +10 and higher. The error ellipses for individual analyses in the concordia diagrams are given at the 2σ level; intercept ages, concordant ages and average values are given at the 95% confidence level (Ludwig, 2001).

Ar-Ar age determinations

Amphiboles with grain size between 0.2 and 0.425 mm were enriched by magnetic and gravimetric means. Sustained hand-picking of the separate led to visual purity. These amphibole samples were irradiated at the McMasters reactor (Hamilton, Ontario, Canada). Ar isotope analyses were performed on a

MAP™ 215-50B rare gas mass spectrometer (at the University of Bern). All isotopes were measured on the Faraday collector. Data listed in tables 4 and 5 were corrected for mass spectrometer background (0.06 fL for mass 36, 0.01 fL for mass 37 and 0.1 fL for mass 39) and discrimination (0.13%/amu favouring heavy masses, determined by measurements of a small pipette open to laboratory air). Furnace blanks always had atmospheric composition and ranged from 0.6 pL at 1000°C to 1 pL at 1500°C; they contained no detectable ^{37}Ar at any temperature. Additional information (e.g. radiogenic ^{40}Ar ($^{40}Ar^*$) concentrations, Cl/Ca and $^{40}Ar^*/^{40}Ar_{tot}$ ratios, etc.) can be easily derived from the data set in Table 5. The interference factors produced by neutron irradiation in the reactor were $(^{39}Ar/^{37}Ar)_{Ca}$=0.00067, $(^{38}Ar/^{37}Ar)_{Ca}$=0.00023, $(^{36}Ar/^{37}Ar)_{Ca}$=0.000255, $(^{40}Ar/^{39}Ar)_{K}$=0.033 and $(^{38}Ar/^{39}Ar)_{K}$=0.0118. Errors in tables 4 and 5 are in-run statistics only and purposefully do not take into account uncertainties of the J gradient, monitor age and decay constants.

Hf isotopes

The Hf-Zr-REE fraction from the U-Pb separation protocol was redissolved and the hafnium was isolated using Eichrom™ Ln-spec resin and measured in static mode on a NuPlasma multi-collector ICP-MS (at ETH Zürich) using a MCN-6000 microconcentric nebuliser for sample introduction. Zircons are commonly characterised by extremely low $^{176}Lu/^{177}Hf$ ratios of less than 0.005 and the $^{176}Hf/^{177}Hf$ were corrected for in-situ radiogenic ingrowth using this ratio. The hafnium ratios were corrected for mass fractionation using a $^{179}Hf/^{177}Hf$ value of 0.7325 and normalised to $^{176}Hf/^{177}Hf$ = 0.282160 of the JMC-475 standard (Blichert-Toft et al., 1997), which was repeatedly measured during analytical sessions. Mean isotopic values are at the 95% confidence level. Epsilon hafnium values were calculated with $^{176}Hf/^{177}Hf_{CHUR}$ = 0.282772 (Blichert-Toft and Albarède, 1997).

BIBLIOGRAPHY

Albarède, F., Simonetti, A., Vervoort, J.D., Blichert-Toft, J. & Abouchami, W. 1998: A Hf-Nd isotopic correlation in ferromanganese nodules. Geophysical Research Letters 25, 3895–3898.

Bard, J.-P., Maluski, H., Matte, P. & Proust, F. 1980: The Kohistan sequence: crust and mantle of an obducted island arc. Geological Bulletin of the University of Peshawar 11, 87–94.

Blichert-Toft, J. & Albarède, F. 1997: The Lu-Hf isotope geochemistry of chondrites and the evolution of the mantle-crust system. Earth and Planetary Science Letters 148, 243–258.

Blichert-Toft, J., Chauvel, C. & Albarède, F. 1997: Separation of Hf and Lu for high-precision isotope analysis of rock samples by magnetic sector multiple collector ICP-MS. Contributions to Mineralogy and Petrology 127, 248–260.

Boulin, J. 1981: Afghanistan structure, Greater India concept and eastern Tethys evolution. Tectonophysics 72, 261–287.

Boutelier, D., Chemenda, A. & Burg, J.-P. 2003: Subduction versus accretion of intra-oceanic volcanic arcs: insight from thermo-mechanical analogue experiments. Earth and Planetary Science Letters 212, 31–45.

Chauvel, C. & Blichert-Toft, J. 2001: A hafnium isotope and trace element perspective on melting of the depleted mantle. Earth and Planetary Science Letters 190, 137–151.

Coward, M.P., Windley, B.F., Broughton, R.D., Luff, I.W., Petterson, M.G., Pudsey, C.J., Rex, D.C. & Khan, M.A. 1986: Collision tectonics in the NW Himalayas. In: Coward, M.P. & Ries, A.C. (Eds.): Collision tectonics. Geological Society Special Publication 19, London, 203–219.

Debon, F., Le Fort, P., Dautel, D., Sonet, J. & Zimmermann, J.L. 1987: Plutonism in western Karakorum and northern Kohistan (Pakistan): a composite Mid-Cretaceous to upper Cenozoic magmatism. Lithos 20, 19–40.

Desio, A., Tongiorgi, E. & Ferrara, G. 1964: On the geological age of some granites of the Karakorum, Hindu Kush and Badakhshan (Central Asia). Proceedings, 22nd International Geological Congress, Delhi Part 11/Section 11, 479–496.

Dietrich, V.J., Frank, W. & Honegger, K. 1983: A Jurassic-Cretaceous island arc in the Ladakh-Himalayas. Journal of Volcanology and Geothermal Research 18, 405–433.

DiPietro, J.A. & Isachsen, C.E. 2001: U-Pb zircon ages from the Indian plate in northwest Pakistan and their significance to Himalayan and pre-Himalayan geologic history. Tectonics 20, 510–525.

Dunlap, W.J. & Wysoczanski, R. 2002: Thermal evidence for early Cretaceous metamorphism in the Shyok suture zone and age of the Khardung volcanic rocks, Ladakh, India. Journal of Asian Earth Sciences 20, 481–490.

Fraser, J.E., Searle, M.P., Parrish, R.R. & Noble, S.R. 2001: Chronology of deformation, metamorphism, and magmatism in the southern Karakoram Mountains. Geological Society of America Bulletin 113, 1443–1455.

Gaetani, M. 1997: The Karakorum Block in Central Asia, from Ordovician to Cretaceous. Sedimentary Geology 109, 339–359.

Gaetani, M. & Garzanti, E. 1991: Multirifting history of North Indian plate margin and NW Himalaya. Bulletin of the American Association of Petroleum Geologists 75, 1397–1414.

Gaetani, M., Le Fort, P., Tanoli, S., Angioli, L., Nicora, A., Sciunnach, D. & Khan, A.M. 1996: Reconnaissance geology in upper Chitral, Baroghil and Karambar districts (northern Karakorum, Pakistan). Geologische Rundschau 85, 683–704.

Gansser, A. 1964: Geology of the Himalayas. Interscience, London, 289 pp.

Gansser, A. 1980: The significance of the Himalayan suture zone. Tectonophysics 62, 37–52.

Godfrey, L.V., Lee, D.C., Sangrey, W.F., Halliday, A.N., Salters, V.J.M., Hein, J.R. & White, W.M. 1997: The Hf isotopic composition of ferromanganese nodules and crusts and hydrothermal manganese deposits: Implications for seawater Hf. Earth and Planetary Science Letters 151, 91–105.

Heuberger, S. (Ed) 2004: The Karakoram-Kohistan Suture Zone in NW Pakistan – Hindu Kush Mountain Range. Geological map and explanatory notes. vdf Hochschulverlag AG, Zürich, 99 pp.

Hildebrand, P.R., Noble, S.R., Searle, M.P., Waters, D.J. & Parrish, R.R. 2001: Old origin for an active mountain range: Geology and geochronology of the eastern Hindu Kush, Pakistan. Geological Society of America Bulletin 113, 625–639.

Honegger, K., Dietrich, V., Frank, W., Gansser, A., Thöni, M. & Trommsdorff, V. 1982: Magmatism and metamorphism in the Ladakh Himalayas (the Indus-Tsangpo Suture Zone). Earth and Planetary Science Letters 60, 253–292.

Kaneko, Y., Katayama, I., Yamamoto, H., Misawa, K., Ishikawa, M., Rehman, H.U., Kausar, A.B. & Shiraishi, K. 2003: Timing of Himalayan ultrahigh-pressure metamorphism: sinking rate and subduction angle of the Indian continental crust beneath Asia. Journal of Metamorphic Geology 21, 589–599.

Khan, T., Khan, M.A., Jan, M.Q. & Naseem, M. 1996: Back-arc basin assemblages in Kohistan, Northern Pakistan. Geodinamica Acta 9, 30–40.

Krogh, T.E. 1973: Low-contamination method for hydrothermal decomposition of zircon and extraction of U and Pb for isotopic age determinations. Geochimica et Cosmochimica Acta 37, 485–494.

Krogh, T.E. 1982a: Improved accuracy of U-Pb zircon dating by selection of more concordant fractions using a high-gradient magnetic separation technique. Geochimica et Cosmochimica Acta 46, 631–635.

Krogh, T.E. 1982b: Improved accuracy of U-Pb zircon dating by the creation of more concordant systems using an air abrasion technique. Geochimica et Cosmochimica Acta 46, 637–649.

Le Fort, P., Michard, A., Sonet, J. & Zimmermann, J.-L. 1983: Petrography, geochemistry and geochronology of some samples from the Karakorum batholith (Northern Pakistan). In: Shams, F.A. (Ed.): Granites of Himalayas, Karakoram and Hindu Kush. Institute of Geology, Punjab University, Lahore, 377–387.

Ludwig, K.R. 2001: Isoplot/Ex, rev. 2.49. A Geochronological Toolkit for Microsoft Excel. Berkeley Geochronology Center, Special Publication No. 1a.

Nowell, G.M., Kempton, P.D., Noble, S.R., Fitton, J.G., Saunders, A.D., Mahoney, J.J. & Taylor, R.N. 1998: High precision Hf isotope measurements of MORB and OIB by thermal ionisation mass spectrometry; insights into the depleted mantle. Chemical Geology 149, 211–223.

Patchett, P.J. & Tatsumoto, M. 1980: Hafnium isotope variations in oceanic basalts. Geophysical Research Letters 7, 1077–1080.
Pearce, J.A., Kempton, P.D., Nowell, G.M. & Noble, S.R. 1999: Hf-Nd element and isotope perspective on the nature and provenance of mantle and subduction components in Western Pacific arc-basin systems. Journal of Petrology 40, 1579–1611.
Pearce, J.A. & Peate, D.W. 1995: Tectonic implications of the composition of volcanic arc magmas. Annual Reviews of Earth and Planetary Sciences 23, 251–285.
Petterson, M.G. & Windley, B.F. 1985: Rb-Sr dating of the Kohistan arc-batholith in the Trans-Himalaya of north Pakistan, and tectonic implications. Earth and Planetary Science Letters 74, 45–57.
Pudsey, C.J. 1986: The Northern Suture, Pakistan: margin of a Cretaceous island arc. Geological Magazine 123, 405–423.
Pudsey, C.J., Coward, M.P., Luff, I.W., Shackleton, R.M., Windley, B.F. & Jan, M.Q. 1985a: Collision zone between the Kohistan arc and the Asian plate in NW Pakistan. Transactions of the Royal Society of Edinburgh: Earth Sciences 76, 463–479.
Pudsey, C.J., Schroeder, R. & Skelton, P.W. 1985b: Cretaceous (Aptian/Albian) age for island-arc volcanics, Kohistan, N Pakistan. Himalayan Geology 3, 150–168.
Rai, H. 1982: Geological evidence against the Shyok Paleosuture, Ladakh Himalaya. Nature 297, 142–144.
Rex, A.J., Searle, M.P., Tirrul, R., Crawford, M.B., Prior, D.J., Rex, D.C. & Barnicoat, A. 1988: The geochemical and tectonic evolution of the central Karakoram, North Pakistan. Philosophical Transactions of the Royal Society of London A 326, 229–255.
Robertson, A.H.F. & Collins, A.S. 2002: Shyok Suture Zone, N Pakistan: late Mesozoic -Tertiary evolution of a critical suture separating the oceanic Ladakh Arc from the Asian continental margin. Journal of Asian Earth Sciences 20, 309–351.
Schaltegger, U., Frank, M. & Burg, J.-P. 2003: A 120 million years record of magmatism and crustal melting in the Kohistan Batholith. Geophysical Research Abstracts; EGS-AGU-EUG Joint Assembly 5, EAE03-A-08307.
Schaltegger, U., Zeilinger, G., Frank, M. & Burg, J.-P. 2002: Multiple mantle sources during island arc magmatism: U-Pb and Hf isotopic evidence from the Kohistan arc complex, Pakistan. Terra Nova 14, 461–468.
Searle, M.P., Khan, A.M., Fraser, J.E., Gough, S.J. & Jan, Q.M. 1999: The tectonic evolution of the Kohistan-Karakoram collision belt along the Karakoram Highway transect, north Pakistan. Tectonics 18, 929–949.
Searle, M.P., Rex, A.J., Tirrul, R., Rex, D.C. & Barnicoat, A. 1989: Metamorphic, magmatic and tectonic evolution of the central Karakoram in the Biafo-Baltoro-Hushe regions of N. Pakistan. In: MALINCONICO, L. & LILLIE, R.J. (Eds.): Tectonics of the Western Himalaya. Geological Society of America, Special Paper 232, 47–74.
Searle, M.P., Windley, B.F., Coward, M.P., Cooper, D.J.W., A.J., R., Rex, D.C., Li, T.D., Xiao, X.C., Jan, M.Q., Thakur, V.C. & Kumar, S. 1987: The closing of Tethys and the tectonics of the Himalaya. Geological Society of America Bulletin 98, 678–701.
Stacey, J.S. & Kramers, J.D. 1975: Approximation of terrestrial lead isotope evolution by a two-stage model. Earth and Planetary Science Letters 26, 207–221.
Stratigraphy, I.C.o. 2004: International stratigraphic chart ICS, IUGS. http://www.stratigraphy.org/chus.pdf.
Tahirkheli, R.A.K., Mattauer, M., Proust, F. & Tapponnier, P. 1979: The India Eurasia Suture Zone in Northern Pakistan: Synthesis and interpretation of recent data at plate scale. In: Farah, A. & De Jong, K.A. (Eds.): Geodynamics of Pakistan. Geological Survey of Pakistan, Quetta, 125–130.
Tapponnier, P., Mattauer, M., Proust, F. & Cassaigneau, C. 1981: Mesozoic ophiolites, sutures and large-scale tectonic movements in Afghanistan. Earth and Planetary Science Letters 52, 355–371.
Thakur, V.C., Virdi, N.S., Rai, H. & Gupta, K.R. 1981: A note on the geology of Nubra-Shyok Area of Ladakh, Kashmir, Himalaya. Journal of the Geological Society of India 22, 46–50.
Tonarini, S., Villa, I.M., Oberli, F., Meier, M., Spencer, D.A., Pognante, U. & Ramsay, J.G. 1993: Eocene age of eclogite metamorphism in Pakistan Himalaya: implications for India-Eurasia collision. Terra Nova 5, 13–20.
Treloar, P.J., Petterson, M.G., Qasim Jan, M. & Sullivan, M.A. 1996: A re-evaluation of the stratigraphy and evolution of the Kohistan arc sequence, Pakistan Himalaya: implications for magmatic and tectonic arc-building processes. Journal of the Geological Society of London 153, 681–693.
Treloar, P.J., Rex, D.C., Guise, P.G., Coward, M.P., M.P., S., Windley, B.F., Petterson, M.G., Jan, M.Q. & Luff, I.W. 1989: K/Ar and Ar/Ar geochronology of the Himalayan collision in NW Pakistan: constraints on the timing of suturing, deformation, metamorphism and uplift. Tectonics 8, 881–909.
Vervoort, J.D., Patchett, P.J., Blichert-Toft, J. & Albarède, F. 1999: Relationships between Lu-Hf and Sm-Nd isotopic systems in the global sedimentary system. Earth and Planetary Science Letters 168, 79–99.
Vervoort, J.D., Patchett, P.J., Gehrels, G.E. & Nutman, A.P. 1996: Constraints on early Earth differentiation from hafnium and neodymium isotopes. Nature 379, 624–627.
Villa, I.M. 2001: Radiogenic isotopes in fluid inclusions. Lithos 55, 115–124.
Villa, I.M., Ruggieri, G. & Puxeddu, M. 1997: Petrological and geochronological discrimination of two white-mica generations in a granite cored from the Larderello-Travale geothermal field (Italy). European Journal of Mineralogy 9, 563–568.
Villa, I.M., Zanchi, A. & Gaetani, M. 2001: Rb-Sr dating of the Tirich Mir pluton, NW Pakistan: pre-140 Ma accretion of the Karakoram terrane to the Asian margin. Journal of Asian Earth Sciences 19/3, supplement 1, 72.
Wijbrans, J. & McDougall, I. 1986: $^{40}Ar/^{39}Ar$ dating of white micas from an Alpine high-pressure metamorphic belt on Naxos (Greece): the resetting of the argon isotopic system. Contributions to Mineralogy and Petrology 93, 187–194.
Woodhead, J.D., Hergt, J.M., Davidson, J.P. & Eggins, S.M. 2001: Hafnium isotope evidence for 'conservative' element mobility during subduction zone processes. Earth and Planetary Science Letters 192, 331–346.
Zanchi, A., Poli, S., Fumagalli, P. & Gaetani, M. 2000: Mantle exhumation along the Tirich Mir Fault (NW Pakistan): Pre-mid-Cretaceous accretion of the Karakorum Terrane to the Eurasian margin. In: Khan, A.M., Treloar, P.J., Searle, M.P. & Jan, M.Q. (Eds): Tectonics of the Nanga Parbat Syntaxis and the Western Himalaya 170. Geological Society, Special Publication, London, 237–252.
Zeilinger, G. 2002: Structural and geochronological study of the Lowest Kohistan Complex, Indus Kohistan region in Pakistan, NW Himalaya. Unpublished PhD, ETH, 243 pp.

Manuscript received September 23, 2005
Revision accepted May 24, 2006
Published Online First May 3, 2007
Editorial Handling: Reto Gieré & Edwin Gnos